Scientific Research Publishing

Open Journal of Geology, 2022, 12, 829-869
https://www.scirp.org/journal/ojg
ISSN Online: 2161-7589
ISSN Print: 2161-7570

# Plio-Quaternary Volcanism in Northeastern Morocco: Petrography and Geochemistry of Outcrops with High Geothermal Potential

**Redouane Meryem[1], Haissen Faouziya[1], Zhang Cong[2], Sadki Othman[3], Raji Mohammed[1]**

[1]LGAGE, Faculty of Sciences Ben Msik, Casablanca, Morocco
[2]Institute of Geology, Chinese Academy of Geological Sciences, Beijing, China
[3]National Office of Hydrocarbons and Mines, Rabat, Morocco
Email: meryem.redouane.2015@gmail.com

**How to cite this paper:** Meryem, R., Faouziya, H., Cong, Z., Othman, S. and Mohammed, R. (2022) Plio-Quaternary Volcanism in Northeastern Morocco: Petrography and Geochemistry of Outcrops with High Geothermal Potential. *Open Journal of Geology*, **12**, 829-869.
https://doi.org/10.4236/ojg.2022.1211040

**Received:** September 22, 2022
**Accepted:** November 4, 2022
**Published:** November 7, 2022



## Abstract

Cenozoic volcanic activity in Morocco started in the Miocene and proceeded, after a short break, during Pliocene and Quaternary. Calc-alkaline magmatic activity occurred first and was accompanied by the eruption of transitional lavas, followed by Plio-Quaternary alkali basaltic activity, which was emplaced within Neogene sedimentary basins of the Rif belt and its foreland. From calc-alkaline to alkaline magmatism, passing through a transitional term, volcanic activities in Morocco formed magnificent outcrops, very diversified in their affinities, their mineral compositions and their geochemistry. The petrographic study and geochemistry of Plio-quaternary volcanic rocks in the areas with high geothermal potential in northeast of Morocco show a dominance of Na-rich basaltic rocks (basanites, basalts, tephrites and basaltic trachy-andesites), followed by trachy-andesites. Most of the samples exhibit an enrichment of large-ion lithophile elements (LILEs) over high-field-strength elements (HFSEs). These results were used to test the global model of Circum-Mediterranean Anorogenic Cenozoic Igneous Province (CiMACI) and the regional model of [1].

## Keywords

Cenozoic, Basaltic Activity, Northeast of Morocco, Alkaline, CiMACI

## 1. Introduction

Neogene-Quaternary volcanic activity is widely present in the Western Mediterranean region, and its volcanic centers and structures are observed all along the Maghrebian coast from Tunisia through Algeria to Morocco [2]-[8].

The study of the west Mediterranean volcanism revealed an evolution in the chemical nature through time [6] [7] [8]. In fact, the first activity was calc-alkaline and was recorded firstly in Algeria and Spain at 16 - 15 Ma, and later (14.5 to 11 Ma) in all Maghrebian margin [5] [6] [9] [10] [11] [12]. This calc-alkaline activity was followed by a potassium-rich shoshonitic to Lamproic activity at 8 - 5 Ma in Spain and 9 - 4 Ma in Africa [2] and lasted by alkaline activity during Plio-quaternay in Spain and earlier from Messinian to quaternary in North Africa [2]. This temporal evolution with the different rocks representing the three volcanic activities can be observed in few volcanic centers such as Oranie in Algeria [7] and Gourougou volcanic field in Morocco [5] [6] [13].

Plio-quaternary volcanism in Morocco is represented by alkali basalts, basanites, basaltic trachy-andesites and other intermediate lava while Miocene volcanism is dominated by calc-alkaline to highly-potassic calc-alkaline and shoshonitic magmas [4] [5] [6] [8] [9] [10] [14] [15] [16] [17] [18]. The transitional magmatism between the calc-alkaline and alkaline activities occurred after the eruption of the first alkali basalt (6.3 Ma) and ceased after the last shoshonitic eruption (4.8 Ma) [8]. In addition to North Africa, where the transitional terms were well described and studied (*i.e.* [4] [5] [6] [19] [20]), the transition from orogenic calc-alkaline magmas to intraplate alkaline associations is frequently observed in many other areas in the Mediterranean region, e.g. in Anatolia and Western Turkey [21], Sardinia [22], Southern Spain [23] and in Central Southern Italy [24].

Different tectonic models were proposed to explain the genesis and the evolution of the different volcanic activities (e.g. [2] [6] [8] [25] [26]). However, the occurrence of a post-collisional magmatic activity close, geographically and temporarily, to an orogenic magmatism is still a hot topic. The main models proposed activities (e.g. [2] [6] [8] [25] [26]) include: 1) an orogenic setting related to subduction for the calcalkaline and the shoshonitic magmatic activity and an intraplate setting for the alkaline activity, contemporaneous with the salinity crisis during the Messinian and involving a westward roll-back of an eastward-dipping slab of the Tethyan oceanic lithosphere; 2) delamination of a part of the continental lithosphere beneath the Alboran Sea; and 3) asthenospheric upwelling (diapirism).

The Plio-quaternary volcanic activity, topic of this paper, is recorded in different structural domains of Morocco, including the Rif belt and the adjacent parts of Eastern Morocco (**Figure 1**). In fact, different volcanic facies mainly basanites and phonolites [27] are observed in the Middle Atlas [18]; in Central Morocco and in the Anti-atlas belt [28]. The Middle Atlas is the largest basaltic province in Morocco and exhibits a hundred of strombolian cones and maars of different ages (Miocene, Pliocene and Quaternary). In the Anti-Atlas, the recent volcanic activity (10 - 2.8 Ma) is represented by the strato-volcano of Siroua to the west, mainly trachytic and Phonolitic with an alkaline to hyper-alkaline character and Jbel Saghro, mostly phonolitic, with olivine-bearing nephelinites,

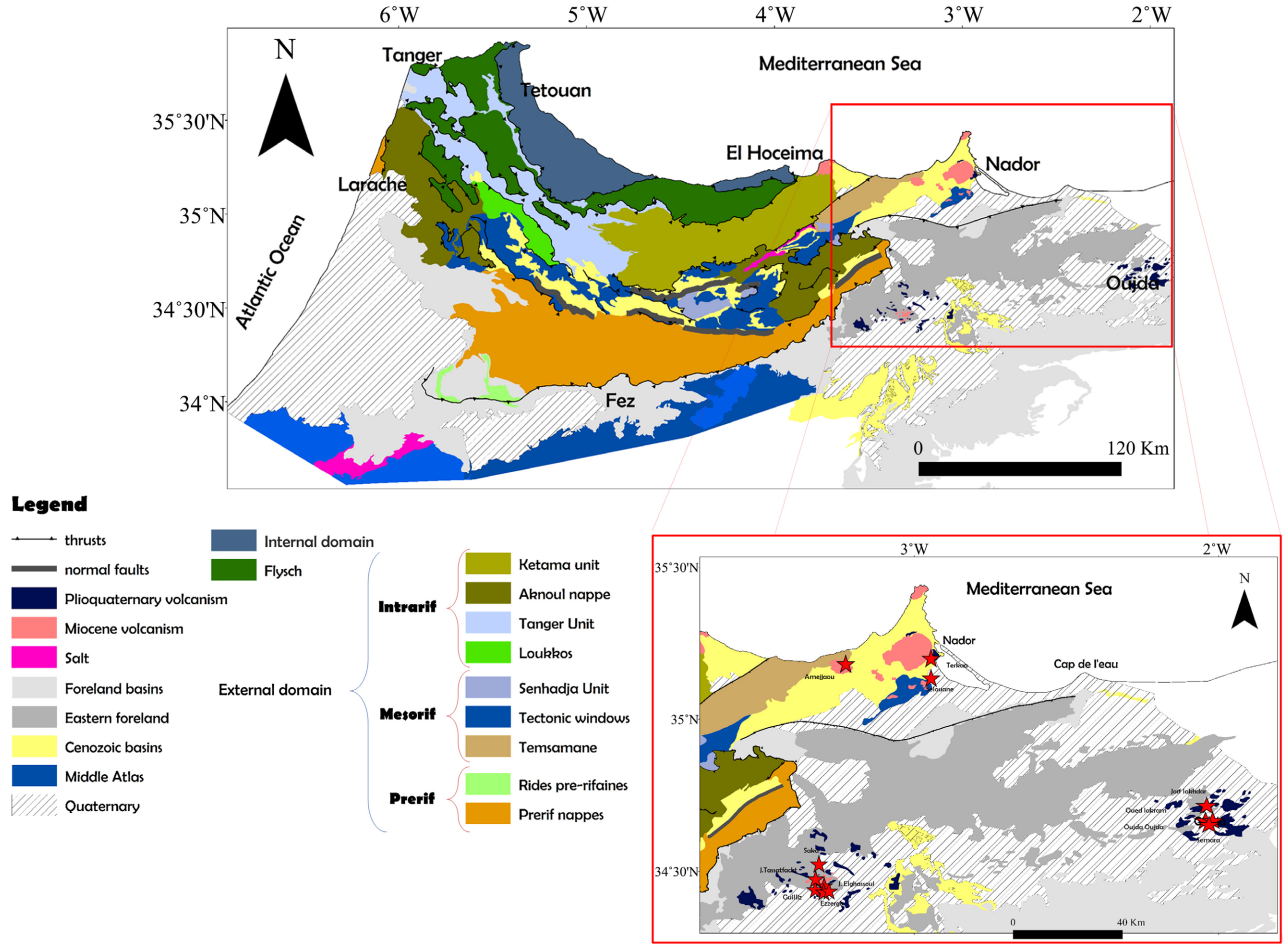


**Figure 1.** Structural map of the north of Morocco (Geological map of Morocco (1/1,000,000)).

phonolitic nephelinites and phonolites, more or less alkaline and similar to the alkali-rocks of Central Morocco [28].

Volcanic areas in northeastern Morocco occur either in the Rif belt's Miocene sedimentary basins or within its foreland (**Figure 1**). The latter is formed by Gareb chaotic units towards the south of the volcanic complex of Gourougou and a part of the deformed tectonic foreland (*i.e.* Beni Bou Yahi and Beni Snassen located in west of Saka and Oujda, respectively). Neogene basins of Guercif and Taourirt-Oujda consist of sediments from middle Miocene to Quaternary, and are connected to the Algerian Tafna basin towards the east [29]. The whole area is affected by faults [30], which crosscut the basement and the overlying cover, and even, locally, the calc-alkaline volcanic rocks [31]. Plio-quaternary volcanic activity in NE of Morocco is noticed to be spatially close to hot water points (springs and wells), with an average geothermal gradient of about 126˚C/km at depths greater than 300 m, as it was recorded by [32] in a borehole near Berkane.

In the present study and in the general frame of constraining the geothermal exploration in the NE of Morocco, different outcrops from the Plio-quaternary activity were studied based on the importance of the heat flow and the permea-

bility within geothermal promising areas. Therefore, we present in this paper the results of new petrology and geochemistry data performed in different volcanic rocks of the northeast of Morocco (Nador, Guilliz, Saka and Oujda areas) with special emphasis on detailed petrography of these rocks, generally missing in the papers already published on this part of Morocco. Furthermore, we intended a comparison of the geochemistry of our rocks with published data of alkali volcanic rocks from different Mediterranean surrounding areas (Middle and Anti-Atlas, Oran, south-eastern Spain and Canary Islands).

## 2. Geological Settings

The Western-Mediterranean alpine belts are considered as the result of a complex orogenic alpine history developed as a consequence subduction processes related to Africa-Eurasia convergence since Cretaceous, the slab roll back of the Maghrebian Tethys lithosphere during the end of Eocene-Early Oligocene and the delamination of the African subcontinental mantle (e.g. [33] [34]). This transition marks the closure of both branches of the Maghrebian Tethys and the opening of the West Mediterranean Basin. The direction of the convergence between Eurasian and African plates is NW-SE [35].

During the Alboran block progressive movement towards the west, the African plate will continue the migration towards the northwest. At the Alboran plate border, the north component creates in its eastern part a sinistral strike-slip zone. The latter will use different tectonic directions emplaced during the collision of the internal zones (Jebha, Nekor etc.) and ensure the opening of the post-nappe basins [2]. From this period and on, the volcanism history of the two provinces (the orogenic and the anorogenic) is discontinuous, the volcanism progression and the opening of basins are symmetrically done from both sides of the strike-slip faulting zone. In Morocco, the opening of Cenozoic basins is shifted towards the East using the directions of older Middle Atlasic accidents, the volcanism follows this progression. In Spain, there is a clear evolution of the volcanism towards the North-west (e.g. [2]).

The Rif belt is situated in the North of Morocco, sketching the southern lamb of the Gibraltar arc and the equivalent of the Betic Cordilleras [36] [37] in the other side of the Mediterranean, and forms the westernmost part of the alpine belt which extends along the north of Africa (with Tell and Kabylie) and continues eastward to Sicily and Calabria in southern Italy. Three main structural domains form the Rif belt, from the North to the South: Internal zones, Flysch Zones and External Zones (**Figure 1**). Each domain is divided itself to several sub-domains as follows:

- Internal zones, also called Alboran domain, where we recognize three main subdomains, which are from the lower to the upper: Sebtides, Ghomarides and the Dorsale calcaire;
- Maghrebian Flyschs; with two main different kinds of Flysch, Numidian, and Mauritanien-Massylian;
- External zones, with three main subdomains and they are from the North to

the South: Intrarif, Mesorif and the Prerif.

The eastern part of the Middle Atlas forms the Rif foreland and consists of high intra-continental belts, notably folded, and characterized by a strong Meso-Cenozoic cover, repetitively affected by a series of tectonic events usually linked to the Alpine orogeny (s.l) [18].

The lithosphere beneath the northeast of Morocco is remarkably thin (15 - 20 km) and the crustal anomaly extends far to the south and draw the so-called "Moroccan hot line" referred to as "MHL", striking NE-SW [25] [38], crossing the main tectonic structures of Central Morocco. The MHL is highlighted by the occurrence of recent volcanic activities along a NE-trending outcrops starting from the Trans-Alboran zone and extending to the Canary Islands. It also covers Atlasic (Middle Atlas and Anti-Atlas) and Riffian domains, from Nador (Gourougou) to Guercif (Guilliz) in the Rif and Oujda areas [2] [6] in the Middle Atlas and Saghro and Siroua in the Anti-Atlas. Geophysical study indicated the presence of high magnetic anomalies beneath the northeast of Morocco, towards the east in the volcanic area [39].

The geochronological data on the northeastern Morocco indicates a temporal evolution of the volcanic activity in this region [6] [8], The oldest record is from the Ras Tarf eruptions (late Tortonian); then the magmatic activity has been interrupted for 2 Ma followed by the Tres Forcas eruptions (North of Gourougou) maintained for almost 0.5 Ma (**Figure 1**). After a short period, eruptions started in Gourougou and Guilliz areas and proceeded for almost 3 Ma. In the Gourougou volcanic field, the volcanic activity has stopped in the early Pliocene and did not resume until Quaternary, while it took longer to reach the surface and record the most recent eruptions in Guilliz area. The volcanic eruptions of Oujda and the alkaline episode of Guilliz emissions were the latest events recorded in the northeastern Morocco.

Based on geochemical (major, REE and isotopes) and geochronological (K/Ar and 40Ar/39Ar) data, many authors concluded to deduce a volcanic evolution in the western Mediterranean area from an orogenic to an intraplate magmatism with the presence of transitional terms (e.g. [2] [8] [40]). In Morocco, the first magmatic activity recorded ranges from calc-alkaline to a highly potassic calc-alkaline and shoshonitic composition. Transitional magmatism occurred between the eruption of the first alkali basalt (6.3 Ma) and the last shoshonitic eruption (4.8 Ma) [8]. The youngest magmatic activity (6.3 - 0.65 Ma) is alkaline represented by basaltic rocks showing an ocean island basalts (OIB) affinity. These rocks are associated with crustal stretching along the trans-current lineaments [41]. This activity was attributed by some authors [42] to the Circum-Mediterranean Anorogenic Cenozoic Igneous Province (CiMACIP).

Samples collected for the present study belong to different outcrops in northeastern Morocco including:

## 2.1. Nador Volcanic Field

Gourougou stratovolcano dominates the landscape near Nador city (**Figure 1** &

Figure 2). This well-preserved stratovolcano and its satellites (9 - 5.4 Ma) are considered the largest volcanic complex in the northeast Morocco. The volcano is of about 12 km diameter and 900 m of elevation and consists mainly of intermediate lava flows. The massif's central part is mostly formed by calc-alkaline and shoshonitic Miocene volcanic rocks (rhyolites, dacites and andesites) in addition to local interstratified volcanoclastic layers with basin sediments [10] and few granodioritic intrusions close to the main volcanic area (Beni Bou Ifrour). In this volcanic field, three areas were studied, Amejjaou and Selouane areas surround the Gourougou stratovolcano from the west and the south, respectively, and Terkaa area is located in the south of the volcanic complex.

Amejjaou volcanic area is located around 12 km in the west of Gourougou's main eruptive centre (Figure 1 & Figure 3) and is crossed by the Nador-Amejjaou village national road. The rocks in both sides of the roads are strongly altered.

Selouane volcanic area is made of two small hills, located 5 km in the southeast of Selouane village, approximately 13 km south of Nador city (Figure 1). Selouane's volcanic rocks are well preserved and very hard to break (Figure 3).

Terkaa volcanic area is located in the southeast of Gourougou's main eruptive centre (Figure 1) and the south of the Terkaa charqiya district. It consists of a large basalt quarry (Figure 4(a)), under current exploitation. The upper volcanic level is vesicular and the vesicles are sometimes filled with marls and calcite.

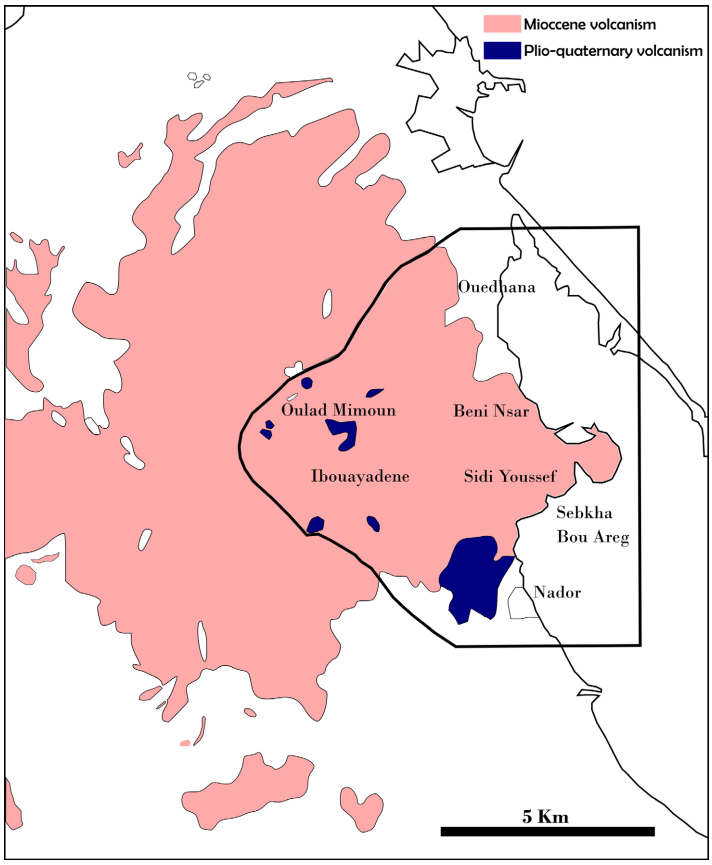


Figure 2. Localization of plioquaternary volcanic rocks in Gourougou volcanic area.

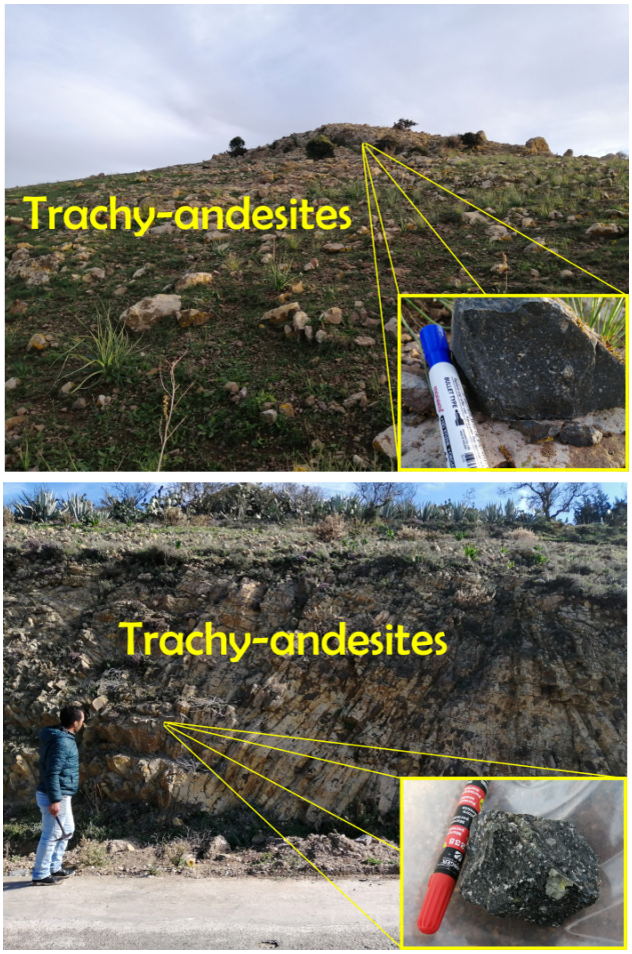


**Figure 3.** Field photos of Selouane and Amejjaou volcanic rocks. (a) Selouane trachy-andesites outcrop; (b) Selouane trachy-andesite sample; (c) Amejjaou trachy-andesites outcrop; (d) Amejjaou trachy-andesite sample.

## 2.2. Saka-Tassatfacht Volcanic Field

In contrast to Ain Zohra volcanic complex, described in the literature [43], hardly seen in the field, Saka's outcrops are well visible and easily accessible (**Figure 4(b)**). Saka volcanic outcrops are located in the north of Guercif city and northeast of the village of Saka. The volcanic area is made of a small hill crosscut by a normal fault oriented NE-SW (**Figure 4(b)**). The rocks are strongly altered and show great similarity with Selouane's volcanic facies.

Tassatfacht is located south of Saka outcrop and consists of greyish basaltic rocks occurring as small blocs and volcanic scree topping the sedimentary levels below (**Figure 4(c)**).

## 2.3. Guilliz Volcanic Field

Guilliz volcanic area is represented as an alignment of volcanic centres, 24 km northeast of Guercif city (located between Fez and Oujda) (**Figure 1**). It consists of two main volcanos (Guilliz Elkbir "big" and Guilliz Essghir "small") and few smaller satellites.

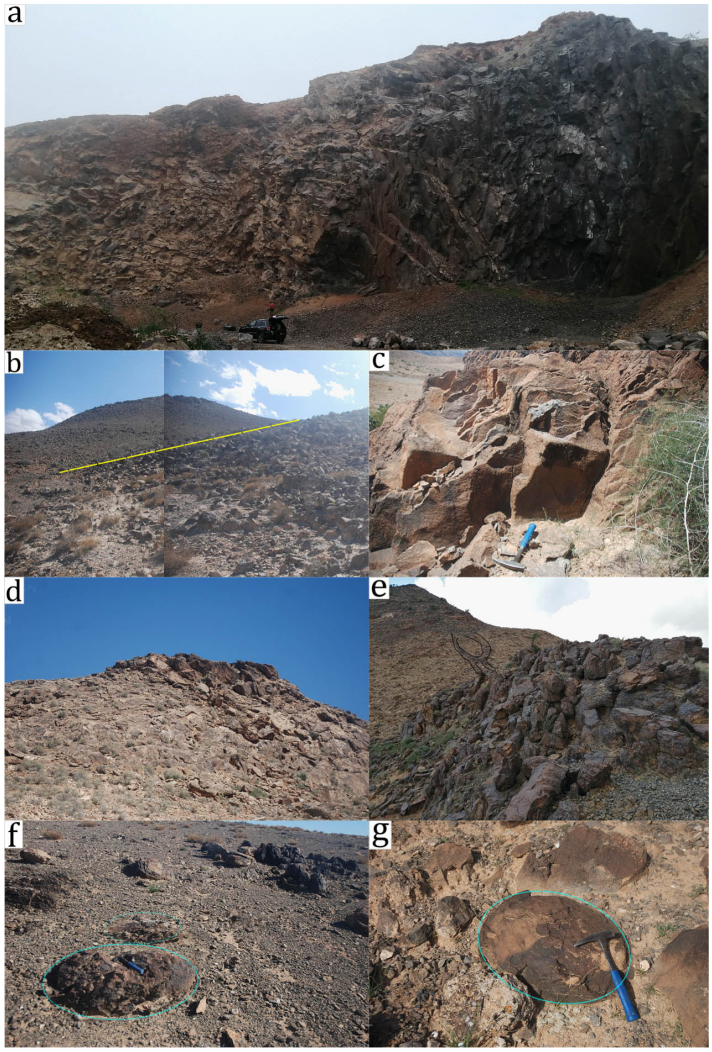


**Figure 4.** Field photos of Terkaa, Saka, Tassatfacht, Guilliz, Elghassoul and Ezzerga volcanic rocks. (a) Terkaa quarry; (b) Saka outcrop crosscut by a normal fault oriented NE-SW; (c) Small basaltic bloc in Tassatfacht; (d) One of the outcrops in the West of Guilliz Elkbir; (e) Basaltic lava flow in Guilliz Essghir; (f) Elghassoul basaltic pillow lavas; (g) Ezzerga spheroidal form in a basaltic outcrop.

The age and the composition of the magmatic flows of Guilliz are similar to those of Gourougou [2]; the evolution goes from more acidic term, calc-alkaline and shoshonitic composition to an under-saturated term of a younger age. The magmatic eruptions occurred within the Neogene Guercif Basin is considered as the eastern continuation of the Riffian foredeep, before getting separated by the late Neogene uplift of the diaper of Tazzeka and it overlies the Jurassic half-grabens of the Middle Atlas [31].

Guilliz Elkbir is the main massif of Guilliz volcanic area and is almost 3 km large; it consists of several felsic outcrops, frequently bearing enclaves and presents irregular forms (**Figure 4(d)**) and sometimes a peculiar shape of domes.

Guilliz Essghir is located in the south of Guilliz Elkbir and it consists of several basaltic flows, some of them are of a great size, while others are thinner and

crosscut other volcanic rocks (**Figure 4(e)**).

### 2.4. Elghassoul-Ezzerga Volcanic Field

This volcanic field crops out in a desertic zone, located in the east of Saka and Guilliz and surrounded by quaternary alluviums from the Tertiary basins (**Figure 1**). The closest geological units to the area are those of the eastern foreland.

Elghassoul volcanic field is presented by two facies; the first is strongly altered, has a greenish colour and exhibits different structures (pillow lava, stratification (N125), and imbrication); the second is less altered and shows no preferential structure (**Figure 4(f)**).

Ezzerga volcanic area outcrops mainly in the valley and is represented by pyroclastic tuffs and lava flows. The rocks are rounded, brecciated, random and compact (**Figure 4(g)**).

### 2.5. Oujda Volcanic Field

Oujda region is a collapsing ditch wedged between the Horsts chain to the south and the Beni Snassen chain to the north (**Figure 1**). This depression was submitted to an intense alkaline volcanic activity which ranging from the upper Neogene (6.2 Ma) to the early Quaternary (1.5 Ma). This depression with about 3.5 to 4 km of diameter is filled with volcanic and volcano-clastic formations deposited in a collapsed area 230 meters deep [44] [45]. This activity also conceals the effects of a phreatomagmatic activity, associated to typical volcanic rocks such as tephrites [6]. The four volcanic areas of Oujda studied within this work are Jorf Lakhdar, Oujda Oujda, Oued Lakram and Semara (**Figure 1**).

Oujda Jorf Lakhdar volcanic area is located in the northwest of Oujda city centre and the outcrop show three different volcanic levels (**Figure 5**). The lowest level is made of spectacular huge volcanic columns, the rocks have a greyish colour and they are well preserved (**Figure 5(a)** & **Figure 7(b)**). The second volcanic level consists of vesicular facies (**Figure 5(c)**), this volcanic level is generally surrounded by marls (**Figure 5(d)**). The third level has the same composition of the first level but the columns are smaller (**Figure 5(f)**).

Oujda-Oujda and Oujda Oued Lakram volcanic areas are small outcrops directly observed on the road named "La Rocade" and they exhibit a variety of structures such as cracks, fractures, breaks (**Figure 6(a)**), secondary alteration minerals filling (**Figure 6(b)** & **Figure 7(c)**) and spheroidal weathering (**Figure 6(f)** & **Figure 7(g)**). Oujda Oued Lakram volcanic rocks are more altered and deformed than those of Oujda Oujda's outcrop (**Figure 6(e)**).

Oujda Semara volcanic area corresponds to an old basalt quarry and is located in the southwest of Oujda city. It is a big outcrop near the national road N17. It consists of three volcanic levels (**Figure 7**); in the middle, it takes a shape of small columns (**Figure 7(a)**), topped by tephrites (**Figure 7(b)**) and topping the lowest level, mostly massif and strongly crosscut by breaks and faults (**Figures 7(c)-(e)**).


**Figure 5.** Field photos of Jorf Lakhdar basaltic structures. (a) Jorf Lakhdar volcanic outcrop; (b) Zoom in the columnar basaltic facies; (c) Zoom in the vesicular facies; (d) Vesicular trachy-andesites surrounded by marls; (e) Zoom in the limit between the vesicular and the marly facies; (f) Columnar basaltic level showing a slight deformation.

## 3. Analytical Methods

Samples are collected from five volcanic fields and they are Nador, Saka-Tassatfacht, Guilliz, Elghassoul-Ezzerga and Oujda. They are generally of a quaternary age, except for one sample from Guilliz volcanic field (Guilliz Elkbir), dated for Miocene and one sample from Nador volcanic field (Amejjaou) where there is no accurate information about the age.

In one hand, whole-rock major elements were analyzed on fused glass disks using X-ray fluorescence (XRF) spectrometer (THERMO ARL ADVANT XP+) at the National Geoanalysis Center, Chinese Academy of Geological Sciences. The results were all normalized against the Chinese rock reference standard GBW07103, GBW07105. Analytical uncertainties range from ±1% to ±5% and the loss on ignition (LOI) was obtained by heating about 1 g of sample powder at 980˚C for 0.5 h [46].

In the other hand, trace elements were analysed at National Geoanalysis Center, Chinese Acedemy of Geological Sciences, using a PerkinElmer Nexion 300D coupled plasma mass spectrometer (ICP-MS) after acid digestion of sample

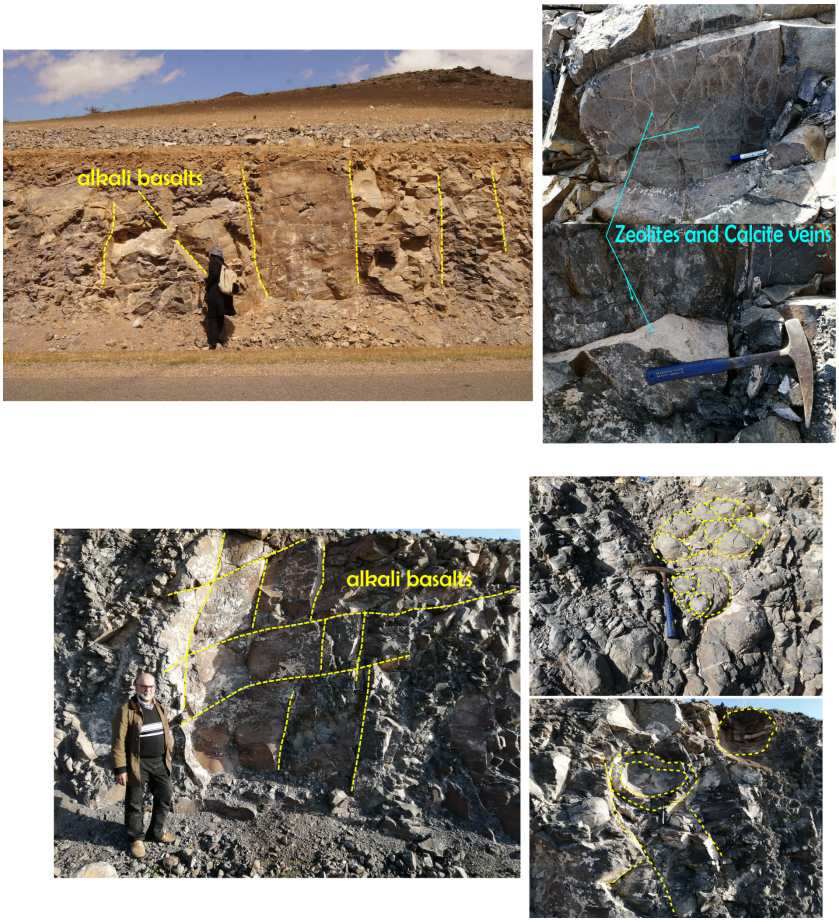


**Figure 6.** Field photos of Oujda-Oujda and Oued Lakram outcrops. (a) Oujda-Oujda outcrop; (b-c) Secondary mineral alteration consisting of Calcite and Zeolite; (d) Oued Lakram outcrop showing an intense cracking; (e-f) Spheroidal weathering of basalts.

powders in Teflon bombs. First, 25 mg of sample was dissolved in an equal mixture of sub-boiling distilled superpure HF and $HNO_3$ with a Teflon digesting vessel on a hot-plate for 24 h. This process was repeated using smaller amounts of acids for another 5 h. Then, the sample was evaporated to incipient dryness, refluxed with 6N $HNO_3$, and heated again to incipient dryness. Finally, the sample was dissolved in 2 ml of 3N $HNO_3$ and diluted with Milli-Q water (18 MΩ) to a final dilution factor of 2000 [47]. The aforementioned Chinese reference rocks (GBW07103 and GBW07105) were also used to monitor the analytical accuracy and precision and the result suggests a relative difference (RE) between measured and recommended values better than 10% for most elements, ±5% for trace elements above 20 ppm, and approximately ±15% for elements below 20 ppm.

Minerals' analyses with SEM were performed at the University IBN ZOHR in Agadir. Selected shells were observed using a JSM IT100 SEM (JEOL) with 0.5 to 30 kV accelerating voltage. Raman Spectroscopic Analysis were conducted by the National Office of Hydrocarbons and Mines laboratory using the Analytical Spectral Device (ASD) NIR "TerraSpec Halo mineral identifier (350 - 2500 nm)".

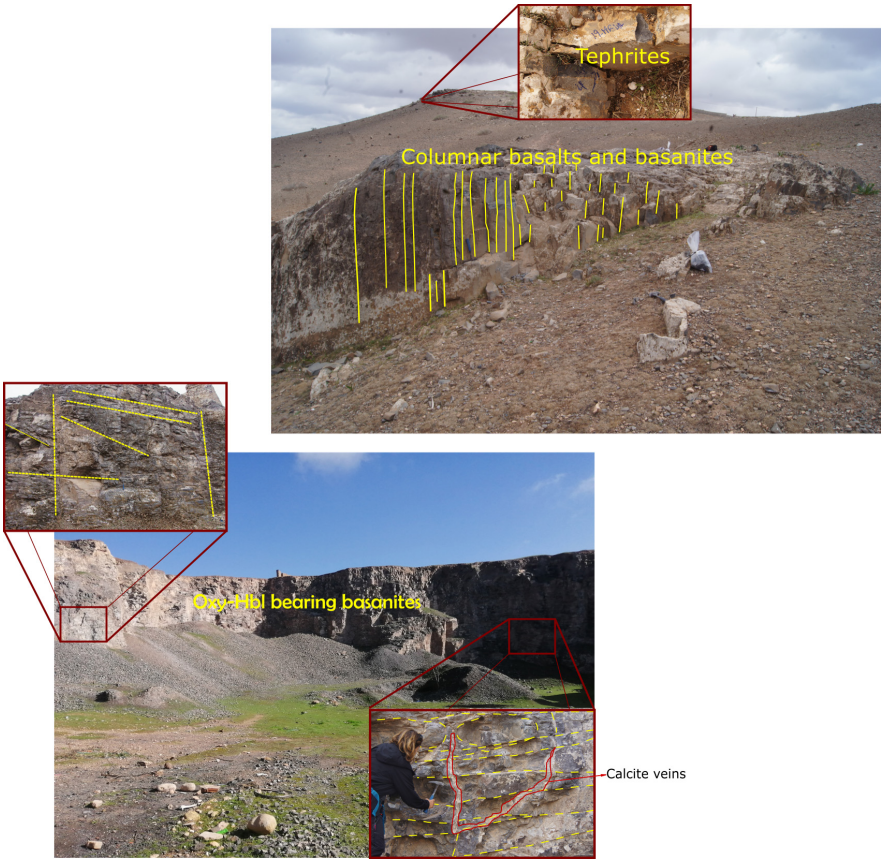


**Figure 7.** Field photos of Semara outcrops. (a) The higher part of Semara outcrop showing columnar basaltic facies; (b) The Uppermost level consisting of tephrites; (c) The lower part of Semara outcrop; (d) Intense cracking with different orientations, generally ranging between N20, N100 and N160; (e) Horizontal cracking and Calcite veins.

## 4. Petrography and Mineralogy

Plio-quaternary volcanic activity in the study area mainly resulted in basaltic rocks such as alkali basalts, basanites and basaltic trachy-andesites, in addition to tephrites and trachy-andesites. The volcanic areas of Jorf Lakhdar, Guilliz Essghir and Amejjaou show a wider petrographic association compared to Terkaa and Tassatfacht volcanic areas, only represented by basaltic trachy-andesites and basanites, respectively.

Basaltic samples have a blueish to greyish colour, they are globally holocrystalline and porphyritic and represent sometimes a glomerophyritic texture. The main phenocrysts occurring in most of the samples are the Olivine (Ol) with different shape and size, Clinopyroxene (Cpx) with a size up to 2 mm, Plagioclase (Pl), Magnetite (Mt) and Amphibole (Amph). The fine-grained groundmass is made of Feldspar (Sanidine (Sa) and Pl), Olivine, Cpx, Mt and accessory minerals such as Sphene and Apatite. Basanite samples consist of a phenocryst assemblage of Ca-rich Plagioclase, Cpx, Olivine, and occasionally few minerals of Leucite (Leu).

Trachy-andesites are generally greyish, inequigranular and porphyritic with a

phenocryst assemblage consisting of Plagioclase, often with an elongated shape, often oriented, Amphibole, Biotite (Bt), Clinopyroxene with a size ranging from 1.5 mm to 0.1 mm, Fe-Ti oxides. The very fine groundmass shows magma mixing prints and small microliths of Pl and Sa. Basaltic trachy-andesites are usually dark in colour, greyish too. They are porphyritic with phenocrysts of poecilitic Plagioclase, Clinopyroxene (up to 3 mm of size, often zoned), Olivine, Iddingsite (Idd) and Magnetite. The groundmass is generally holocystalline, mainly made of intergranular or interstitial textures, with local mineral orientations but sometimes, an aphanitic groundmass is recorded.

Basanites and tephrites are usually Si-poor alkali facies, they mainly consist of Pyroxenes (Opx and Cpx), Amphibole, Pl, very few Ol, Idd and Mt.

### 4.1. Nador Volcanic Field

In this volcanic field and as our study is focused mainly on Plio-quaternary volcanic activity, three volcanic outcrops were sampled and studied: Terkaa, Selouane and Amejjaou.

Terkaa is made for the major part of basaltic trachy-andesites (**Figure 8**). They are porphyric with a very fine-grained groundmass. The phenocrysts assemblage consists of Cpx (Augite) (**Figures 8(a)-(c)** & **Figure 9(a)**) + Ol (**Figure 8(b)**) + Amp (Oxy-Hbl) + Pl (zoned) (**Figure 9(b)**) + Idd (**Figure 8(b)**) + Mt (**Figure 8(d)**), with few small crysts of KF (**Figure 8(a)**).

Amejaou is made of basanites, basalts and trachy-andesites (**Figure 8**). They are generally porphyric and exhibit a phenocrysts assemblage of Bt (deformed) (**Figures 8(a)** & **Figure 9(d)**) + Amp (oxy-Hbl) (**Figure 8(b)**) + Pl (An = 50 - 60, Andesine, frequently zoned) (**Figure 8(c)** & **Figure 9(e)**) + KF + Cpx (fractured Aegyrinic augite and augite) (**Figure 8(d)** & **Figure 9(c)**) + Lm + Mt inclusions (**Figure 8(d)**). They show a fine-grained groundmass, sometimes blurry with few microliths (**Figure 8**).

Selouane is made of basaltic trachy-andesites. They are porphyric with a fine-grained groundmass and present a phenocrysts assemblage of Pl (zoned) + Ol + Idd + Bt + KF + Mt (**Figure 8(d)**).

### 4.2. Saka-Tassatfacht Volcanic Field

Saka outcrop is well preserved and is mainly formed by basalts and trachy-andesites. Both facies have a porphyric microlithic texture. Microliths occupy the most of basaltic rocks' mineral content and they generally consist of Pl (**Figure 10(a)**). They also exhibit a phenocryst assemblage of Cpx (Augite) and OPx (**Figures 10(b)-(d)**) + Ol + Idd (**Figure 10(d)**) + Pl (**Figure 10(e)**) + Mt, while the trachy-andesites show the same mineral assemblage excluding Ol and adding + KF phenocrysts.

Tassatfacht volcanic rocks consist of basanites. They are porphyric and exhibit a fine-grained groundmass. The phenocryst assemblage consists of zoned Cpx (Mg-rich) (**Figure 9(f)**) + Ol + Idd + Pl (**Figure 10(f)**) + Mt (**Table 1**).

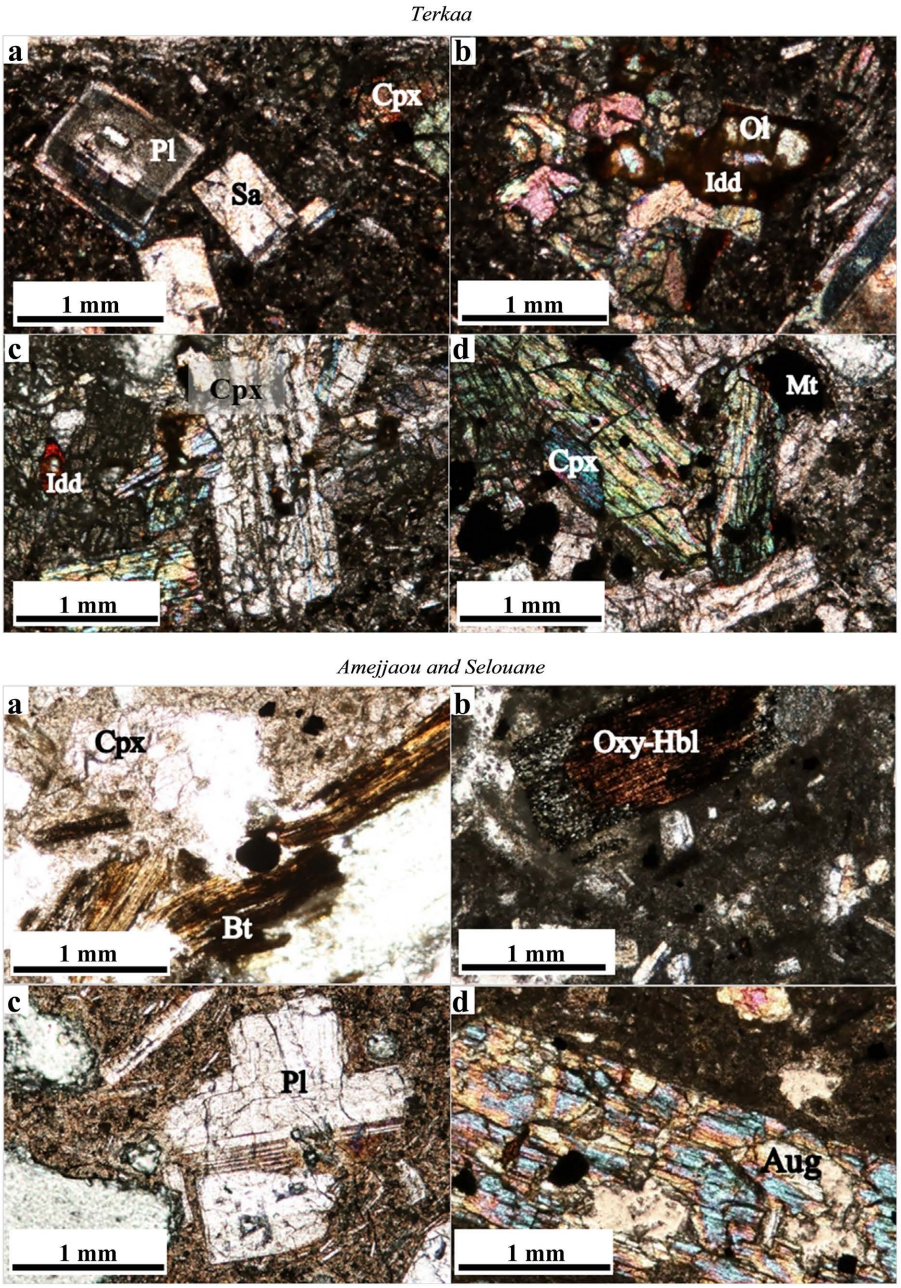


**Figure 8.** Petrography of Terkaa, Amejjaou and Selouane outcrops. Terkaa: Basaltic trachy-andesite showing (a) phenocrysts of Feldspar in a fine-grained groundmass; (b) Iddingsitized Olivine; (c) Intersected phenocrysts of CPx; (d) Imbricated CPx and Mt. Amejjaou and Selouane: (a) Scattered and deformed Bt in basanite; (b) Oxy-Hbl in a trachy-andesite; (c) Intersected phenocrysts of Pl in basalt; (d) Augite phenocryst presenting inclusions (Mt and Idd) in a trachy-andesite.

### 4.3. Guilliz Volcanic Field

Located in the North of Guercif, two different volcanic activities were recorded. The most recent activity crops out in Guilliz Essghir, while Guilliz Elkbir is mainly dominated by the older (Miocene) volcanic activity, except for few random eruptions.

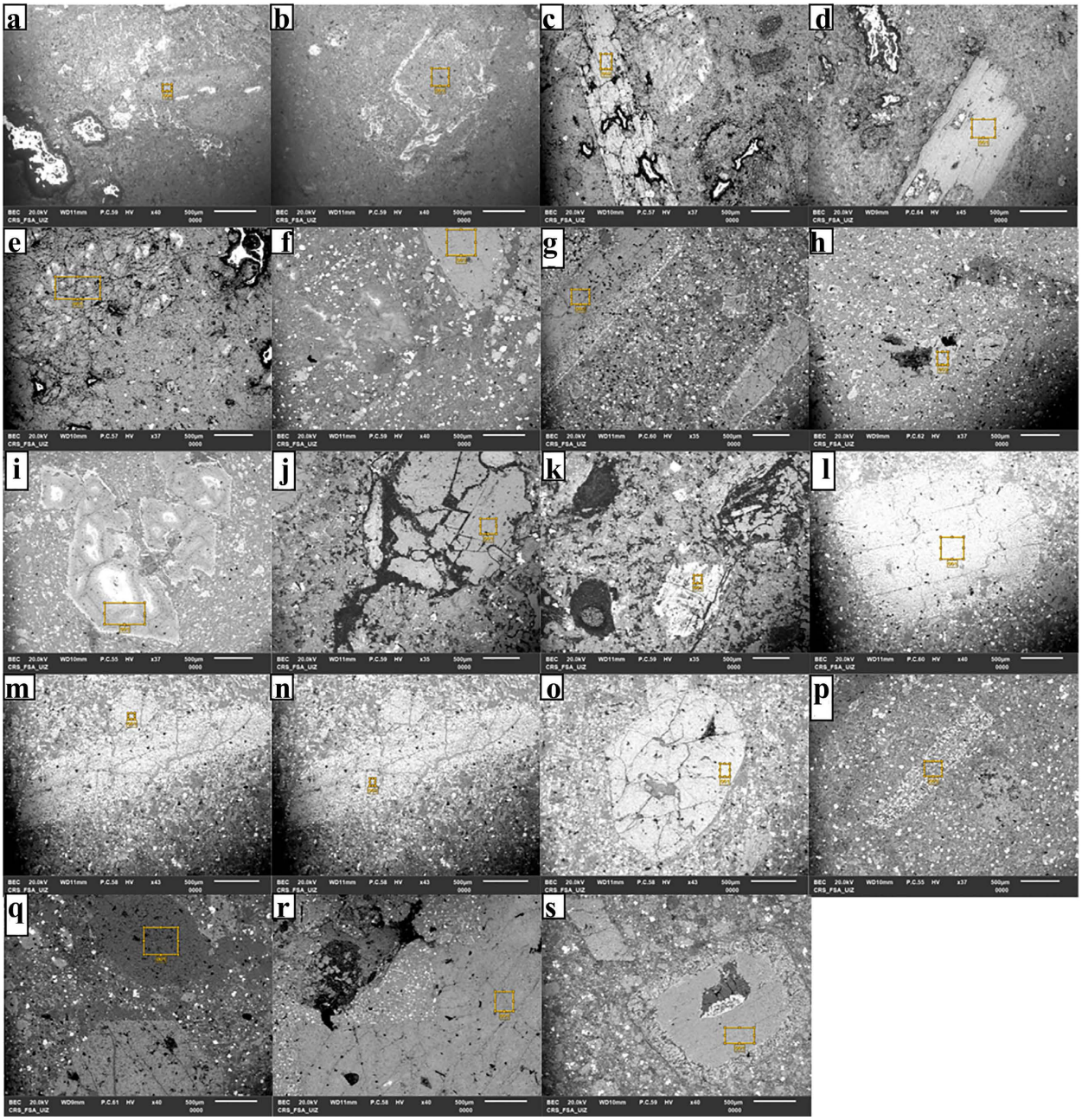


**Figure 9.** MEB of different phenocrysts from the volcanic areas. (a) Cpx in Terkaa; (b) Zoned plagioclase more calcic towards the centre in Terkaa; (c) Augite (Mg rich) in Amejjaou; (d) Biotite in Amejjaou; (e) Pl in Amejjaou; (f) Cpx in Tassatfacht; (g) Cpx (Mg-rich) in Ezzerga; (h) Cpx in Guilliz Essghir; (i) Olivine (Fo) in Guilliz Essghir; (j) Calcite in Guilliz Elkbir; (k) Oxy-Hbl of Guilliz Elkbir; (l) Oxy-Hbl Jorf Lakhdar; (m) Cpx Jorf Lakhdar; (n) Oxy-Hbl Jorf Lakhdar; (o) Olivine (Fo) Jorf Lakhdar; (p) Oxy-Hbl Semara; (q) Leucite in Semara; (r) Pl in Oujda Oued lakram; (s) Oxy-Hbl in Oujda-Oujda with a Ferric rim.

Guilliz Essghir is made of alkali basalts, basaltic trachy-andesites and basanites. They are microlithic porphyric with a phenocryst assemblage of Pl (Figure 11(a)), frequently zoned (labradorite-andesine) and exhibiting different mineral inclusions (Sph + Mt + Idd) + Cpx (Figure 9(h); Figure 11(b); Figure 11(d) & Figure 11(e)) + Lim + Ol (Figure 9(I); Figure 11(c) & Figure 11(f)) + KF (Figure 11(e)), with an abundance of secondary minerals (Zeo + Cal) (Figure 11).

*Saka and Tassatfacht*

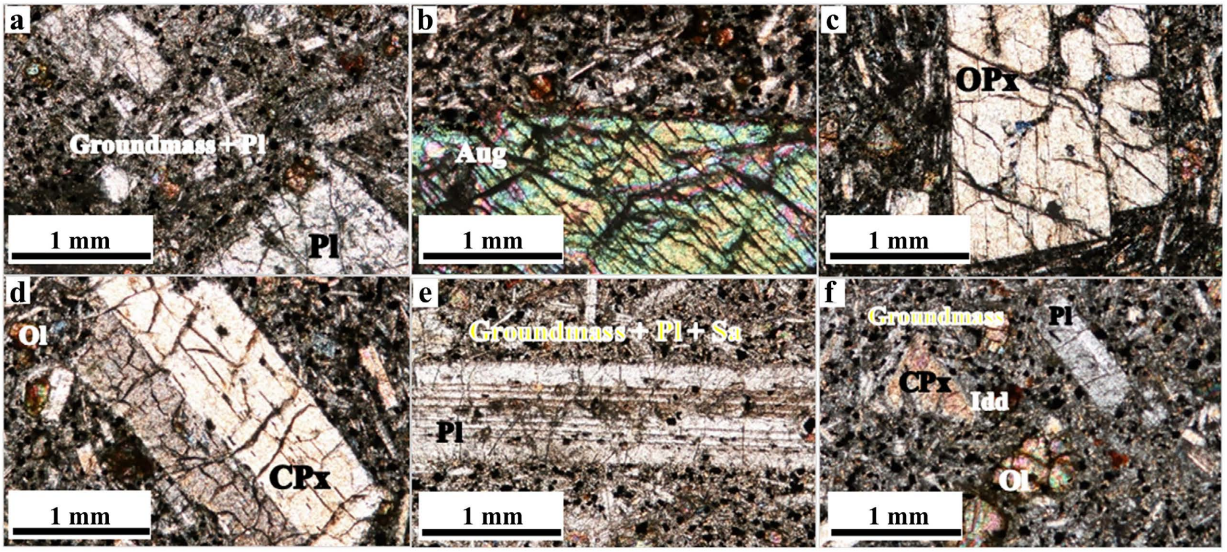


**Figure 10.** Petrography of Saka-Tassatfacht volcanic rocks. (a) Intersected microliths of Pl in basalt; (b) Augite phenocryst in basalt; (c) Opx phenocryst in basalt; (d) CPx phenocryst in basalt with small altered Ol; (e) Long phenocryst of Pl showing Mt inclusions in basalt; (f)Phenocrysts of Pl, altered Ol and Cpx phenocrysts surrounded by a fine-grained groundmass.

**Table 1.** Corresponding MEB analysis.

| Samples/bulk elements (%) | Mineral | C | $Na_2O$ | MgO | $Al_2O_3$ | $SiO_2$ | Cl | $K_2O$ | CaO | $TiO_2$ | FeO | $P_2O_5$ | MnO |
|---|---|---|---|---|---|---|---|---|---|---|---|---|---|
| a | Cpx | 19.69 | 0.96 | 9.38 | 12.11 | 32.6 | 0.2 | 5.35 | 0.98 | 4.72 | 14 | - | - |
| b | Pl | 42.83 | 2.02 | - | 21.12 | 27.23 | 0.07 | 0.25 | 6.48 | - | - | - | - |
| c | Aug | 19.11 | 0.54 | 11.57 | 1.14 | 44.87 | 0.11 | - | 16.71 | - | 5.95 | - | - |
| d | Bt | 20.15 | 0.93 | 11.78 | 11.21 | 32.71 | 0.38 | 6.91 |  | 3.79 | 12.14 | - | - |
| e | Pl | 26.84 | 4.1 | - | 21.96 | 37.14 | 0.22 | 0.59 | 8.38 | - | 0.77 | - | - |
| f | Cpx | 12.14 | 0.83 | 12.33 | 7.37 | 42.79 | - | - | 18.21 | 1.61 | 4.73 | - | - |
| g | Cpx | 15.44 | 1.37 | 13 | 13.02 | 30.96 | 0.13 | 6.63 | 3.74 | 6.92 | 8.37 | 0.41 | - |
| h | Cpx | 18.71 | - | 22.17 | 1.15 | 33.07 | - | - | 1.17 | 0.51 | 23.21 | - | - |
| i | Ol | 16.6 | - | 39.1 | - | 36.53 | - | - | - | - | 7.77 | - | - |
| j | Cal | 21.23 | 1.5 | 0.68 | 0.85 | 3.14 | - | - | 72.59 | - | - | - | - |
| k | Oxy-Hbl | 23.62 | 1.34 | 4.06 | 3.86 | 24.24 | 0.16 | 0.93 | 2.8 | 0.83 | 36.4 | 0.69 | 1.06 |
| l | Oxy-Hbl | 11.19 | 1.03 | 15.44 | 14.11 | 33.95 | - | 8.11 | 0.86 | 7.14 | 8.17 | - | - |
| m | Cpx | 21.3 | 1.14 | 32.16 | 0.56 | 33.86 | 0.27 | 0.19 | 0.8 | 0.3 | 9.42 | - | - |
| n | Oxy-Hbl | 22.09 | 1.24 | 26.14 | 2.34 | 33.09 | 0.25 | 0.48 | 1.48 | 0.32 | 12.57 | - | - |
| o | Ol | 16.35 | 1.03 | 10.86 | 7.38 | 40.29 | - | - | 17.08 | 2.35 | 4.47 | - | - |
| p | Oxy-Hbl | 26.59 | 4.83 | 4.39 | 13.2 | 30.27 | - | 3.01 | 1.81 | 3.62 | 12.73 | - | - |
| q | Leu | 18.74 | 2.01 | 0.35 | 18.56 | 46.57 | 0.32 | 5.3 | 7.8 | - | - | 0.35 | - |
| r | Pl | 13.96 | 2.46 | - | 31.92 | 37.63 | - | - | 13.73 | - | - | 0.3 | - |
| s | Oxy-Hbl | 6.89 | - | 17.09 | 14.81 | 35.89 | - | 9.03 | - | 7.65 | 8.63 | - | - |

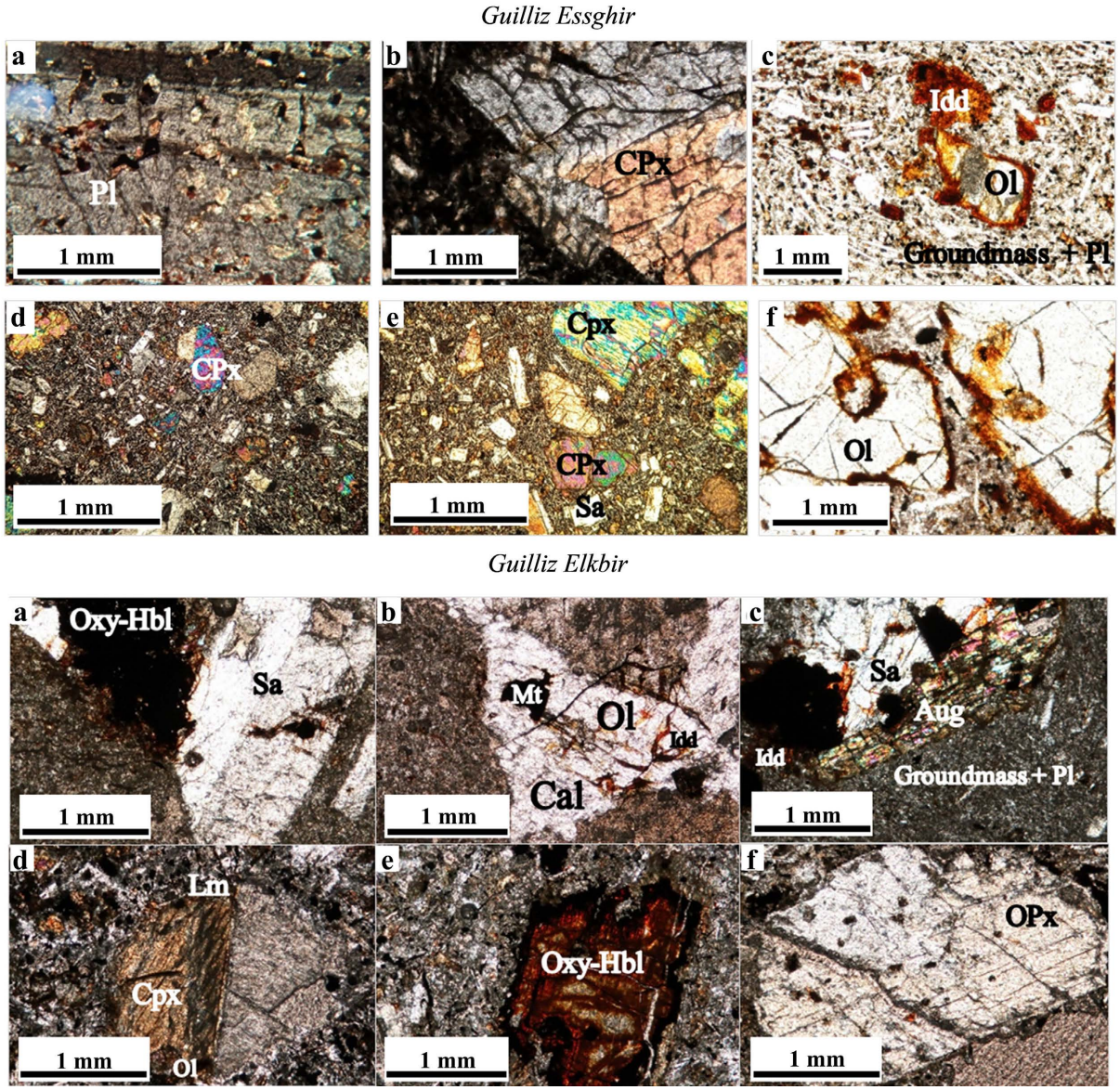


**Figure 11.** Petrography of Guilliz volcanic area. Guilliz Essghir: (a) Huge phenocryst of Pl in a basalt, exhibiting inclusions of Mt and Idd; (b) CPx phenocryst in a basalt; (c) Altered Ol phenocrysts in a microlithic groundmass of a basalt; (d) CPx phenocrysts in a fine-grained groundmass of a basaltic trachy-andesite; (e) CPx and Sa phenocrysts in basaltic trachy-andesite; (f) Huge altered Ol phenocrysts in a basanite. Guilliz Elkbir: trachy-andesites showing: (a) Sa and Oxy-Hbl phenocrysts surrounded by a fine-grained groundmass; (b) Agglomerates of Mt, Ol, Idd and Cal; (c) Imbricated phenocrysts of Sa, Aug and altered Ol; (d) Altered CPx phenocryst; (e) Oxy-Hbl phenocryst; (f) OPx phenocryst.

Guilliz Elkbir consists of trachy-andesites. They are porphyric with a fine-grained groundmass (**Figure 11(a)** & **Figure 11(b)**) and show a phenocryst assemblage of KF (zoned) (**Figure 11(a)** & **Figure 11(c)**) + Cpx (Augite and Aegyrinic Augites) (**Figure 11(c)** & **Figure 11(d)**) + Oxy-Hbl (**Figure 9(k)** & **Figure 11(e)**) + Opx (**Figure 11(f)**) + Lim + Mt + Cal (**Figure 9(j)** & **Figure 11(b)**).

### 4.4. Elghassoul-Ezzerga Volcanic Field

Elghassoul and Ezzerga volcanic outcrops are made of alkali basalts. They are

porphyric with a fine-grained groundmass (Figure 12(a) & Figure 12(b)). The phenocryst assemblage consists of Ol + Idd (Figure 12(a)) + Cpx (Augite) (Figure 9(g) & Figure 12(c)) + Pl (zoned) + KF + Mt + Cal + Zeo (Figure 12(d)). However, they represent some mineralogical differences: basaltic rocks of Elghassoul show phenocrysts of Opx (Figure 12(e)) and secondary minerals of zeolites and calcite, while Ezzerga basalts exhibit phenocrysts of Oxy-Hbl (Figure 12(b)) with a microlithic groundmass (Figure 12(f)).

### 4.5. Oujda Volcanic Field

Oujda volcanic areas considered in this study are all located in the east, north-east and northwest of the city. Jorf Lakhdar outcrop is made of basaltic trachy-andesites, basalts and basanites. Four different facies have been identified, the first level is porphyric with a fine-grained to microlithic groundmass while the other levels show only few phenocrysts with dominance of the fine-grained groundmass. The first volcanic level shows a phenocryst assemblage of Ol (Figure 13(a)) + Idd (Figure 13(b)) + Pl (Figure 13(c)) + Oxy-Hbl (Figure 9(l); Figure 9(n) & Figure 13(d)) + Cpx (Figure 9(m) & Figure 13(e)) + Mt + KF with a secondary alteration of Calcite (Figure 13(f)). The second volcanic level is rather microlithic with only KF and Mt crysts. The third volcanic level exhibits a phenocryst assemblage of rare Ol + Idd + KF + Mt, with zeolite and calcite secondary minerals (Figure 9(o) & Figure 13(f)). The fourth level (the uppermost) shows a poor phenocryst assemblage of Cpx + Lm + Idd + Pl + KF + Mt.

Semara outcrops are made of basanites and tephrites, three different levels are presented in the field. The lowest level exhibit a porphyric aphanitic texture (Figure 13(a)) with a phenocryst assemblage of Oxy-Hbl (Figure 9(p) & Figure 13(b)) + Ol (Figure 13(c)) + Cpx (Figure 13(d)) + Idd (Figure 13(e)) + Pl + Mt, with

*Elghassoul and Ezzerga*

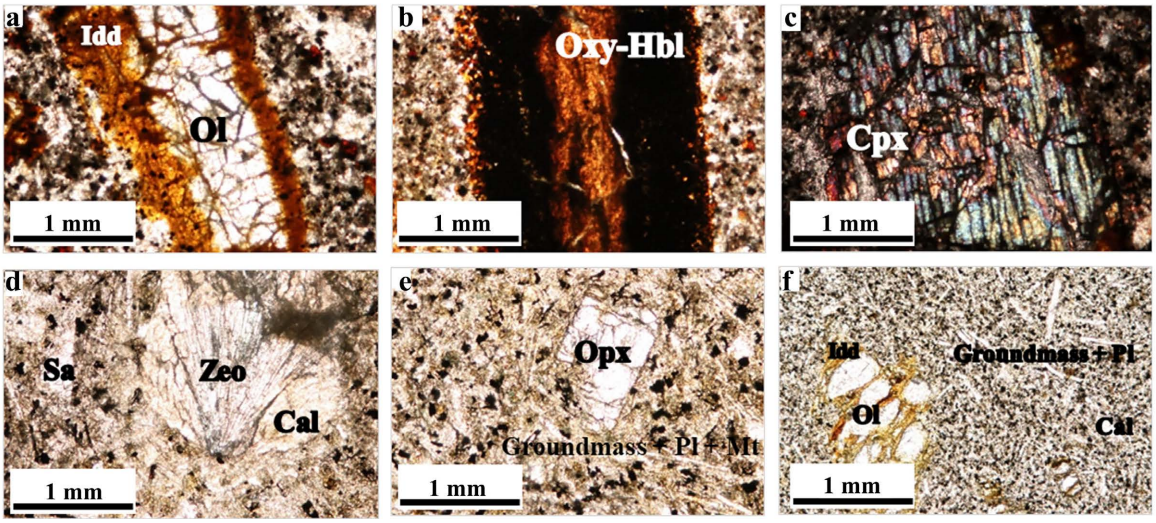


Figure 12. Petrography of Elghassoul-Ezzerga basalts showing some huge phenocrysts. (a) Altered Ol Phenocrysts; (b) Oxy-Hbl phenocryst; (c) CPx phenocryst; (d) Hydrothermal alteration minerals (Zeolite and Calcite); (e) OPx phenocryst in a microlithic groundmass; (f) Altered Ol Phenocrysts in a microlithic groundmass.

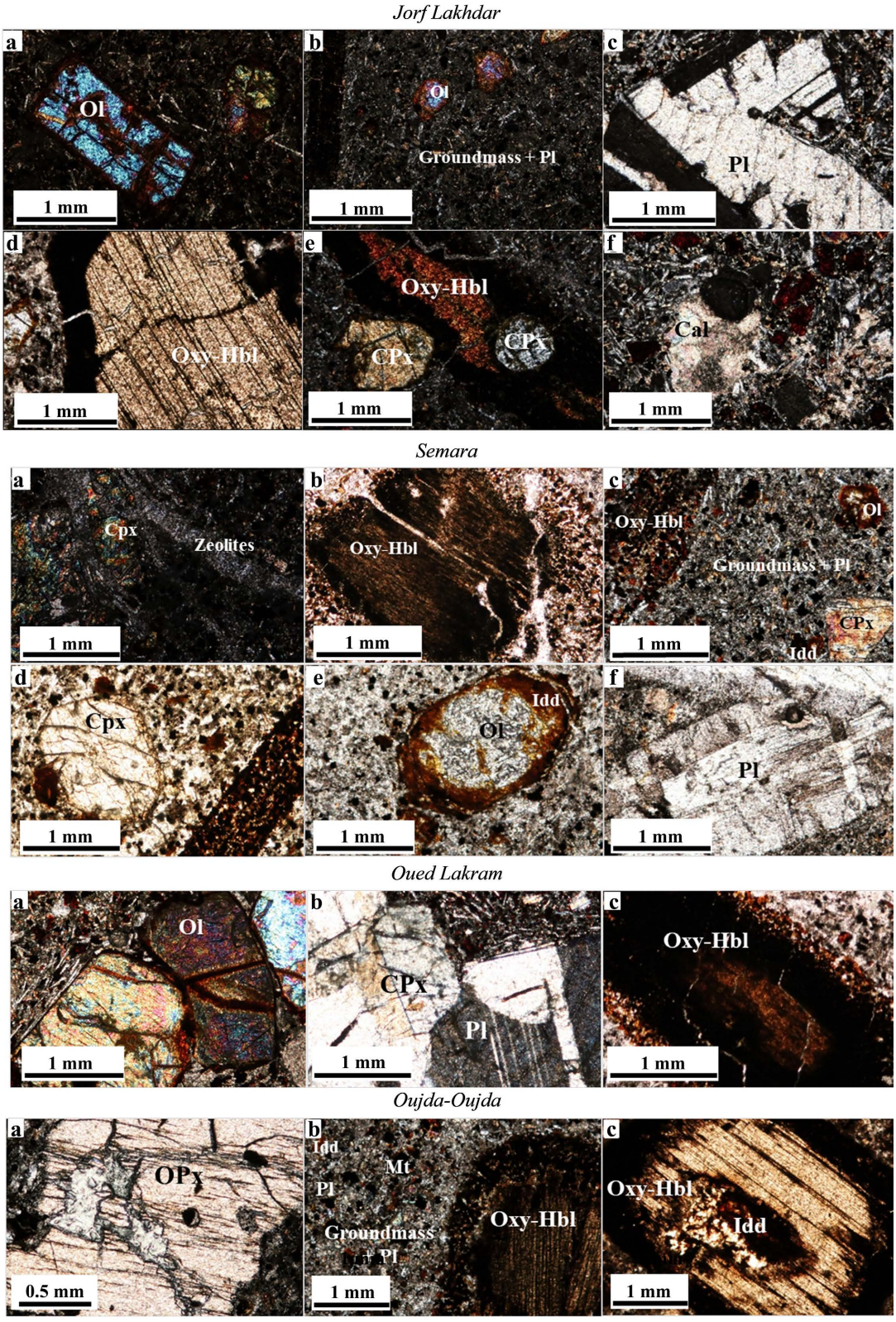


**Figure 13.** Petrography of volcanic rocks of Oujda. Jorf Lakhdar: (a) Ol phenocrysts; (b) Altered Ol in a fine-grained groundmass; (c) Imbricated Pl phenocrysts; (d) Huge Oxy-Hbl phenocryst surrounded by a thick ferric rim; (e) A cracked Oxy-Hbl phenocryst crossed by to rounded Cpx phenocrysts; (f) Calcite alteration in a microlithic groundmass. (Continued on the next page)

the same secondary minerals of Zeolites and Calcites (Figure 13(b)). The level in the middle shows less phenocrysts, mainly consisting of Cpx + KF + Leu (Figure 9(q)) + Mt, with Pl showing traces of the magma mixing process (Figure 13(f)). The third level shows a fine-grained groundmass with rare small phenocrysts of Pl + Idd + Mt.

Oued Lakram and Oujda-Oujda volcanic fields outcrop in both sides of the road taken from the West of Oujda to Guenfouda in the South. Oued Lakram area mainly consists of alkali basalts with intensely altered intrusions. They are porphyric with a fine-grained groundmass and exhibit a phenocryst assemblage of zoned Ol (Figure 13(a)) + Idd + Pl (mostly oriented and intersected) (Figure 9(r) & Figure 13(a) & Figure 13(b)) + Cpx (Figure 13(b)) + Lim + Bt (as relics) + Mt + KF + Oxy-Hbl (Figure 13(c)). Secondary minerals are of Zeolites and Calcite. The oxidized volcanic intrusion consists of altered porphyric basalts with few phenocrysts of Ol + Idd + KF + Pl + Mt.

Oujda-Oujda outcrop is made of basanites and tephrites; it presents different local volcanological and deformation structures (e.g. radial form and frequent fracturing lineaments). They are porphyric with a fine-grained groundmass. They show a phenocryst assemblage of pyroxenes with rare Opx (Figure 13(a)) and Cpx + oxy-Hbl (Figure 13(b)), surrounded by a thick ferric rim (Figure 9(s)) and exhibiting Idd inclusions (Figure 13(c)) + KF + Pl in addition to secondary Carbonates mineral.

The clinopyroxenes are generally Mg-rich, Ca and Ti content is highly relevant in the sampled phenocrysts. However, sometimes they exhibit a high content of Fe. Overall samples, plagioclase is Ca-rich and olivine is Mg-rich. Oxy-hbl show high contents of Mg, Fe, Ti and K (Table 1).

## 5. Major- and Trace-Element Geochemistry

We selected 19 Rock samples from different volcanic field from Eastern Morocco to be analysed at the National Geoanalysis Center, Chinese Aceadmy of Geological Sciences. Major-element compositions of $SiO_2$, $Al_2O_3$, $Fe_2O_3$, MgO, CaO, $Na_2O$, $K_2O$, $TiO_2$, $P_2O_5$, MnO were analyzed by X-ray fluorescence (XRF). Trace elements of Li, Be, Sc, Ti, V, Cr, Mn, Co, Ni, Cu, Zn, Ga, Ge, As, Rb, Sr, Y, Zr, Nb, Mo, Cd, In, Sn, Sb, Cs, Ba, La, Le were analyzed by inductively coupled plasma mass spectrometry (ICP-MS). The analyzed rock types included different petrographic types from basalt to trachy-andesite. The whole-rock major- and trace-element data for the analyzed samples are presented in Table 2 & Table 3.

### 5.1. Hydrothermal Alteration Effects

Analyzed rock samples display slight to moderate alteration effects, as reflected in their loss on ignition (LOI) values, ranging mainly between 0.34 and 3.05 wt% (Table 1) and in their petrographic assemblages.

Petrographic observations indicate that all the samples exhibit a replacement of olivine with iddingsite suggesting an oxidizing environment during the alteration

**Table 2.** Whole rock major element chemical data of the studied samples from the northeast of Morocco.

| Sample | MR-7 | MR-9 | MR-28 | MR-31 | MR-34 | MR-36 | MR-39 | MR-40 | MR-45 | MR-46 |
|---|---|---|---|---|---|---|---|---|---|---|
| Location | Jorf Lakhdar | | Oujda Oujda | | Jorf Lakhdar | | Terkaa | | Saka | |
| Rock type | basaltic trachy-andesite | basalt | tephrite | basanite | basanite | trachy-andesite | basaltic trachy-andesite | basaltic trachy-andesite | basalt | trachy-andesite |
| $SiO_2$ | 53.19 | 45.46 | 44.72 | 42.46 | 42.45 | 45.75 | 52.85 | 53.04 | 45.52 | 58.97 |
| $TiO_2$ | 1.91 | 2.40 | 3.60 | 3.51 | 3.65 | 2.38 | 1.00 | 0.98 | 2.37 | 0.81 |
| $Al_2O_3$ | 18.99 | 16.88 | 16.34 | 15.03 | 14.41 | 16.63 | 17.28 | 16.87 | 16.75 | 17.05 |
| $TFe_2O_3$ | 8.24 | 11.00 | 12.30 | 12.18 | 11.83 | 10.51 | 8.02 | 7.91 | 10.51 | 5.30 |
| MnO | 0.22 | 0.16 | 0.21 | 0.20 | 0.18 | 0.16 | 0.13 | 0.12 | 0.16 | 0.06 |
| MgO | 2.24 | 3.99 | 5.95 | 5.20 | 7.17 | 6.39 | 3.66 | 3.46 | 6.19 | 1.65 |
| CaO | 5.51 | 10.14 | 9.36 | 9.67 | 9.50 | 9.32 | 7.48 | 7.23 | 9.37 | 5.68 |
| $Na_2O$ | 4.03 | 2.92 | 3.90 | 3.78 | 3.47 | 3.12 | 3.05 | 3.04 | 3.02 | 2.88 |
| $K_2O$ | 3.73 | 1.74 | 3.50 | 1.10 | 0.72 | 1.60 | 3.12 | 3.29 | 1.47 | 3.48 |
| $P_2O_5$ | 0.83 | 0.44 | 0.81 | 0.79 | 0.63 | 0.51 | 0.39 | 0.39 | 0.50 | 0.45 |
| LOI | 1.97 | 2.12 | 1.27 | 3.05 | 2.92 | 0.99 | 0.66 | 0.80 | 0.94 | 0.89 |
| SUM | 100.85 | 97.26 | 101.96 | 96.97 | 96.92 | 97.34 | 97.64 | 97.11 | 96.79 | 97.21 |

| Sample | MR-12 | MR-13 | MR-16 | MR-18 | MR-19 | MR-20 | MR-41 | MR-42 | MR-44 |
|---|---|---|---|---|---|---|---|---|---|
| Location | Guilliz Elkbir | Tassatfacht | Guilliz Essghir | | | | | Amejjaou | |
| Rock type | trachy-andesite | basanite | basalt | basalt | basanite | basaltic trachy-andesite | basanite | trachy-andesite | basalt |
| $SiO_2$ | 59.28 | 44.44 | 47.09 | 45.09 | 42.26 | 51.70 | 43.56 | 59.96 | 45.58 |
| $TiO_2$ | 1.27 | 1.49 | 1.72 | 1.68 | 2.11 | 1.84 | 2.34 | 0.85 | 2.38 |
| $Al_2O_3$ | 16.39 | 16.07 | 16.56 | 15.69 | 16.33 | 18.26 | 13.54 | 17.37 | 16.59 |
| $TFe_2O_3$ | 6.80 | 9.85 | 10.11 | 10.90 | 9.70 | 7.99 | 13.19 | 5.44 | 10.70 |
| MnO | 0.13 | 0.14 | 0.17 | 0.16 | 0.15 | 0.23 | 0.16 | 0.06 | 0.16 |
| MgO | 1.75 | 5.90 | 6.77 | 8.57 | 4.39 | 2.15 | 7.40 | 1.73 | 6.40 |
| CaO | 3.76 | 12.59 | 8.73 | 9.81 | 7.91 | 5.46 | 8.07 | 5.43 | 9.14 |
| $Na_2O$ | 4.57 | 2.74 | 3.51 | 2.97 | 3.42 | 3.96 | 3.34 | 2.90 | 2.86 |
| $K_2O$ | 3.77 | 0.64 | 1.26 | 0.77 | 1.77 | 4.11 | 2.34 | 3.47 | 1.85 |
| $P_2O_5$ | 0.39 | 0.21 | 0.37 | 0.26 | 0.56 | 0.79 | 0.95 | 0.46 | 0.50 |
| LOI | 0.53 | 0.77 | 0.83 | 0.34 | 1.49 | 3.37 | 2.35 | 2.29 | 0.98 |
| SUM | 98.65 | 94.83 | 97.12 | 96.25 | 90.09 | 99.86 | 97.25 | 99.96 | 97.13 |

processes (Figures 11-13). Vesicles and fractures in studied samples are filled with secondary minerals, mainly calcite and zeolite, probably resulting from the circulation of hot hydrothermal fluids. In alkali systems, zeolites in vesicles dissolve with decreasing temperature, and F.K. precipitates.

**Table 3.** Whole rock trace element chemical data of the studied samples from the northeast of Morocco.

| Sample | MR-7 | MR-9 | MR-28 | MR-31 | MR-34 | MR-36 | MR-39 | MR-40 | MR-45 | MR-46 |
|---|---|---|---|---|---|---|---|---|---|---|
| Location | Jorf Lakhdar | | Oujda Oujda | | Jorf Lakhdar | | Terkaa | | Saka | |
| Rock type | basaltic trachy-andesite | basalt | tephrite | basanite | basanite | trachy-andesite | basaltic trachy-andesite | basaltic trachy-andesite | basalt | trachy-andesite |
| Li | 18.70 | 8.68 | 8.61 | 8.91 | 10.70 | 18.50 | 10.00 | 8.90 | 7.95 | 8.08 |
| Be | 3.12 | 1.45 | 2.58 | 2.64 | 2.22 | 3.39 | 2.76 | 2.68 | 1.59 | 1.74 |
| Sc | 5.8 | 22.3 | 18.9 | 20.3 | 26.4 | 6.6 | 24.5 | 23.2 | 23.8 | 22.8 |
| Ti | 11,289 | 14,387 | 19,698 | 20,114 | 20,770 | 10,724 | 6013 | 5535 | 14,353 | 14,692 |
| V | 76 | 330 | 402 | 408 | 388 | 76 | 234 | 229 | 351 | 364 |
| Cr | 19.8 | 66.3 | 30.7 | 16.4 | 90.1 | 2.3 | 61.8 | 57.0 | 77.3 | 72.2 |
| Mn | 1760 | 1318 | 1608 | 1647 | 1418 | 1733 | 972 | 856 | 1286 | 1308 |
| Co | 10.20 | 39.40 | 40.40 | 38.70 | 44.70 | 11.80 | 25.70 | 29.00 | 43.80 | 43.50 |
| Ni | 9.42 | 37.50 | 35.20 | 32.40 | 67.70 | 4.63 | 27.80 | 23.80 | 49.20 | 49.40 |
| Cu | 8.10 | 37.20 | 42.40 | 45.50 | 48.40 | 7.32 | 55.20 | 46.70 | 40.40 | 36.60 |
| Zn | 105.0 | 91.8 | 107.0 | 119.0 | 109.0 | 105.0 | 61.9 | 49.4 | 90.9 | 98.6 |
| Ga | 20.1 | 19.1 | 21.2 | 21.7 | 21.2 | 21.2 | 17.6 | 16.1 | 19.6 | 20.6 |
| Ge | 1.17 | 1.12 | 1.13 | 1.16 | 1.21 | 1.19 | 1.12 | 1.08 | 1.12 | 1.18 |
| As | 1.16 | 1.22 | 1.16 | 2.16 | 1.19 | 1.11 | 1.35 | 1.98 | 0.90 | 0.96 |
| Rb | 109.0 | 42.6 | 120.0 | 124.0 | 64.4 | 114.0 | 124.0 | 125.0 | 36.0 | 43.0 |
| Sr | 1151 | 670 | 1030 | 1121 | 999 | 1047 | 602 | 513 | 847 | 742 |
| Y | 36.1 | 23.5 | 28.2 | 29.5 | 26.1 | 37.6 | 21.2 | 19.9 | 21.1 | 21.2 |
| Zr | 397 | 143 | 332 | 343 | 292 | 416 | 126 | 117 | 132 | 137 |
| Nb | 145.0 | 43.3 | 157.0 | 159.0 | 124.0 | 154.0 | 32.2 | 30.5 | 50.4 | 51.0 |
| Mo | 1.59 | 2.95 | 3.47 | 3.50 | 2.41 | 1.52 | 0.85 | 1.06 | 1.70 | 1.67 |
| Cd | 0.17 | 0.20 | 0.13 | 0.15 | 0.13 | 0.17 | 0.07 | 0.05 | 0.12 | 0.21 |
| In | 0.08 | 0.07 | 0.09 | 0.10 | 0.09 | 0.08 | 0.04 | 0.04 | 0.07 | 0.07 |
| Sn | 2.56 | 1.72 | 2.48 | 2.62 | 2.56 | 2.70 | 1.51 | 1.78 | 1.69 | 1.81 |
| Sb | 0.11 | 0.10 | 0.15 | 0.14 | 0.13 | 0.17 | 0.11 | 0.19 | 0.10 | 0.12 |
| Cs | 1.13 | 0.77 | 2.02 | 2.26 | 1.81 | 2.14 | 1.58 | 2.22 | 2.63 | 2.78 |
| Ba | 1056 | 562 | 893 | 837 | 1039 | 1120 | 893 | 775 | 646 | 653 |
| La | 85.8 | 32.5 | 88.0 | 82.6 | 66.4 | 90.6 | 39.0 | 41.8 | 38.5 | 39.4 |
| Ce | 165.0 | 61.5 | 174.0 | 166.0 | 134.0 | 177.0 | 67.6 | 72.0 | 72.8 | 74.4 |

| Sample | MR-12 | MR-13 | MR-16 | MR-18 | MR-19 | MR-20 | MR-41 | MR-42 | MR-44 |
|---|---|---|---|---|---|---|---|---|---|
| Location | Guilliz Elkbir | Tassatfacht | Guilliz Essghir | | | | | Amejjaou | |
| Rock type | trachy-andesite | basanite | basalt | basalt | basanite | basaltic trachy-andesite | basanite | trachy-andesite | basalt |
| Li | 19.00 | 7.29 | 7.08 | 4.77 | 7.59 | 6.32 | 8.73 | 8.25 | 12.20 |

**Continued**

| | | | | | | | | | |
|---|---|---|---|---|---|---|---|---|---|
| Be | 3.47 | 1.57 | 1.52 | 0.98 | 1.40 | 1.00 | 4.10 | 4.46 | 2.32 |
| Sc | 13.5 | 24.1 | 23.3 | 29.0 | 22.6 | 34.9 | 23.1 | 23.9 | 24.6 |
| Ti | 7360 | 15,158 | 10,394 | 9582 | 13,070 | 8850 | 5158 | 4950 | 5329 |
| V | 96 | 358 | 209 | 230 | 240 | 263 | 200 | 186 | 199 |
| Cr | 11.1 | 85.7 | 185.0 | 256.0 | 25.8 | 191.0 | 25.1 | 26.7 | 27.0 |
| Mn | 1032 | 1390 | 1373 | 1199 | 1261 | 1189 | 398 | 444 | 947 |
| Co | 25.20 | 47.50 | 42.40 | 46.60 | 35.70 | 45.60 | 17.90 | 19.90 | 20.30 |
| Ni | 5.88 | 52.70 | 87.20 | 116.00 | 32.70 | 100.00 | 8.00 | 8.66 | 6.53 |
| Cu | 8.88 | 40.50 | 40.80 | 42.30 | 34.90 | 54.00 | 8.27 | 8.35 | 6.69 |
| Zn | 69.5 | 96.1 | 84.2 | 77.4 | 81.7 | 77.5 | 48.9 | 44.7 | 60.8 |
| Ga | 21.5 | 20.1 | 18.3 | 16.8 | 18.3 | 17.5 | 19.9 | 20.6 | 18.6 |
| Ge | 1.37 | 1.22 | 1.16 | 1.09 | 1.13 | 1.11 | 1.50 | 1.45 | 1.41 |
| As | 1.78 | 1.22 | 0.78 | 0.61 | 4.29 | 0.55 | 4.38 | 4.61 | 2.90 |
| Rb | 121.0 | 20.7 | 27.5 | 18.1 | 52.1 | 14.1 | 151.0 | 165.0 | 79.2 |
| Sr | 329 | 908 | 583 | 474 | 710 | 495 | 616 | 616 | 386 |
| Y | 38.4 | 22.2 | 22.6 | 19.8 | 25.4 | 20.0 | 21.1 | 23.2 | 23.3 |
| Zr | 281 | 134 | 128 | 96 | 125 | 93 | 197 | 213 | 125 |
| Nb | 66.8 | 50.9 | 41.1 | 23.8 | 67.9 | 19.5 | 17.2 | 18.1 | 11.5 |
| Mo | 3.12 | 1.63 | 1.84 | 0.94 | 1.90 | 0.83 | 0.46 | 0.52 | 0.48 |
| Cd | 0.12 | 0.14 | 0.11 | 0.10 | 0.11 | 0.05 | 0.01 | 0.01 | 0.05 |
| In | 0.06 | 0.08 | 0.07 | 0.07 | 0.08 | 0.07 | 0.07 | 0.06 | 0.04 |
| Sn | 2.99 | 1.68 | 1.45 | 1.17 | 1.37 | 1.15 | 3.94 | 3.92 | 1.66 |
| Sb | 0.27 | 0.08 | 0.08 | 0.15 | 0.10 | 0.06 | 0.51 | 0.57 | 0.27 |
| Cs | 2.13 | 2.83 | 1.41 | 0.39 | 1.44 | 0.30 | 11.90 | 13.80 | 7.55 |
| Ba | 694 | 655 | 391 | 222 | 696 | 193 | 1679 | 1616 | 751 |
| La | 66.1 | 40.2 | 31.1 | 18.2 | 42.0 | 14.8 | 49.1 | 56.5 | 35.8 |
| Ce | 126.0 | 74.0 | 55.6 | 35.0 | 72.1 | 28.8 | 92.1 | 108.0 | 65.9 |

To constrain the nature of the main alteration phases present in these rocks, analysis by Raman Spectroscopy of basaltic rocks from Oujda Semara and Guilliz Essghir show that the main hydrothermal alteration is a-clay type, followed by mica-type, oxides, carbonates and sulfates minerals (Table 4). Abundant minerals such as calcite, zeolite (Analcime) were also observed in thins sections. Calcite is observed in basalts and pyroclastic tuffs due to the high porosity in the lava (Figure 12 and Figure 13). The argillic alteration is characterized by the presence of montmorillonite, palygorskite, stilpnomelane and ferrimontmorillonite, eventually accompanied by low-temperature zeolites (Table 4).

The mica-type zone develops up to temperatures of 160˚C, above which montmorillonite becomes unstable. Montmorillonite is a dioctahedral smectite that

**Table 4.** Hydrothermal alteration minerals in Plio-quaternary basaltic rocks of NE of Morocco depicted by Raman Spectroscopy.

| Clays | Phyllosilicates | Oxides | Carbonates | Sulfates |
|---|---|---|---|---|
| Vermiculite | Muscovite | Hematite | Calcite | Jarosite |
| Iron Smectite | Sepiolite | | | |
| Iron Saponite | Palygorskite | Goethite | | |
| KaolinitePX | Stilpnomelane | | | |
| | Montmorillonite | | | |
| | Ferrimontmorillonite | | | |

usually occurs in argillic alteration facies and it is a typical product of hydrolysis reactions using silicate phases (Pl, F.K, Px, Ol, volcanic glass), generally at temperature below 160˚C (**Figure 14**). Kaolinite is a very common dioctahedral alteration mineral that we find in superficial geothermal zones and it is the first alteration clay mineral to form but it is not considered as a good thermal indicator, unlike the montmorillonite, systematically present in every hydrothermal setting. Both minerals generally indicate a low temperature domain and less frequently even medium temperature (*i.e.* Montmorillonite in Philippines [48]).

Sepiolite and palygorskite alteration minerals are mainly recorded in mafic and ultramafic rocks of oceanic crust. They generally reflect a hydrothermal temperature below 160˚C (**Figure 14**) and are locally found in argillic alteration facies [49]). Although they are not totally phyllic minerals, they are usually referred to as phyllosilicate s.l. [50]. Palygorskite might also be an indicator of a temperature close to 200˚C [51].

Saponite and Vermiculite are tetrahedral smectites; the former is frequently identified within high temperature hydrothermal zones (propylitic facies) of active geothermal systems [52]. While the latter is substantially is typically found in argillic hydrothermal alteration facies. Kaolinite is a mineral of intermediate argillic alteration facies and can rarely occur in developed argillic facies [53]. Its significance lays on indicating relatively low fluid temperature (<110˚C) (**Figure 14**).

The presence of jarosite indicates the probable presence of shallow sulphides. The occurrence of kaolinite and jarosite might indicate a boundary between oxidized and reduced materials and hence, point to acid-sulphate conditions surrounding the sulphides [54].

As the hydrothermal alteration minerals are quite various and exhibit large compositional variation, we believe that more than one hydrothermal fluid is implicated in the alteration process after the volcanic activity volcanic setup. Alteration minerals can be classified based on temperature range in two classes into two classes: a high temperature hydrothermal fluid of and a medium to low temperature thermal fluid. The first is responsible of the precipitation of oxides and sulphates, while the latter has controlled the clay, micas and calcite alteration.

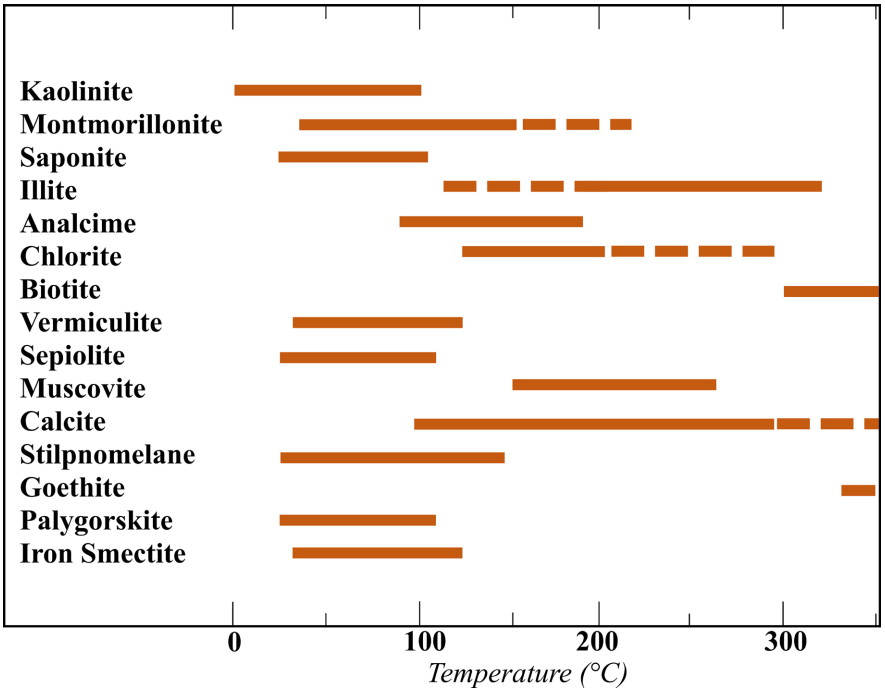


**Figure 14.** Temperature spectra for different hydrothermal alteration minerals.

## 5.2. Major and Trace Geochemistry

Given this range of variations in the LOI values, we recalculated the major-element oxides to total 100% on a volatile-free basis before using these compositions in classification geochemical diagrams. In the TAS classification diagram of [55], the volcanic rock samples plot in the basalts, basanites, basaltic trachy-andesites, trachy-andesites and tephrites fields (**Figure 15**). In the TAS diagram, all the samples are plot in between alkaline-subalkaline separating line of [56]. Basaltic trachy-andesites (samples MR-7, MR-20, MR-39 and MR-40) contain $SiO_2$ (51.7 - 53.19 wt%), and $K_2O + Na_2O$ (6.17 - 8.07 wt%). Basalts (samples MR-9, MR-16, MR-18, MR-36, MR-44 and MR-45) contain $SiO_2$ (45.09 - 47.09 wt%), and $K_2O + Na_2O$ (3.75 - 4.77 wt%). Basanites (samples MR-13, MR-19, MR-31, MR-34 and MR-41) contain $SiO_2$ (42.26 - 44.72 wt%), and $K_2O + Na_2O$ (3.38 - 5.68 wt%). The tephrite sample (MR-28) contain $SiO_2$ (44.72 wt%), and $K_2O + Na_2O$ (7.4 wt%). Finally, the most felsic facies of trachy-andesites (samples MR-12, MR-42 and MR-46) containing $SiO_2$ (58.97 - 59.96 wt%), and $K_2O + Na_2O$ (6.36 - 8.34 wt%). Except for samples MR-20, MR-39, MR-40, MR-42 and MR-46 who show a negative $Na_2O/K_2O$ values, all the samples have a sodic affinity.

To summarize, the studied volcanic outcrops consist only on mafic rocks (basalts, basanites and tephrites) as for example Oujda-Oujda and Tassatchaft, others as Terkaa, only by intermediate rocks while other volcanic field exhibit rocks spanning from mafic to felsic rocks as for example Amejjaou and Guiliz Esghir and Jorf Lakhder. Saka volcanic field is formed only by trachy-andesite.

The multiple plot of $SiO_2$ vs. other major elements diagrams depict the following trends (**Figure 16**) basaltic trachy-andesite samples show high $Al_2O_3$ and

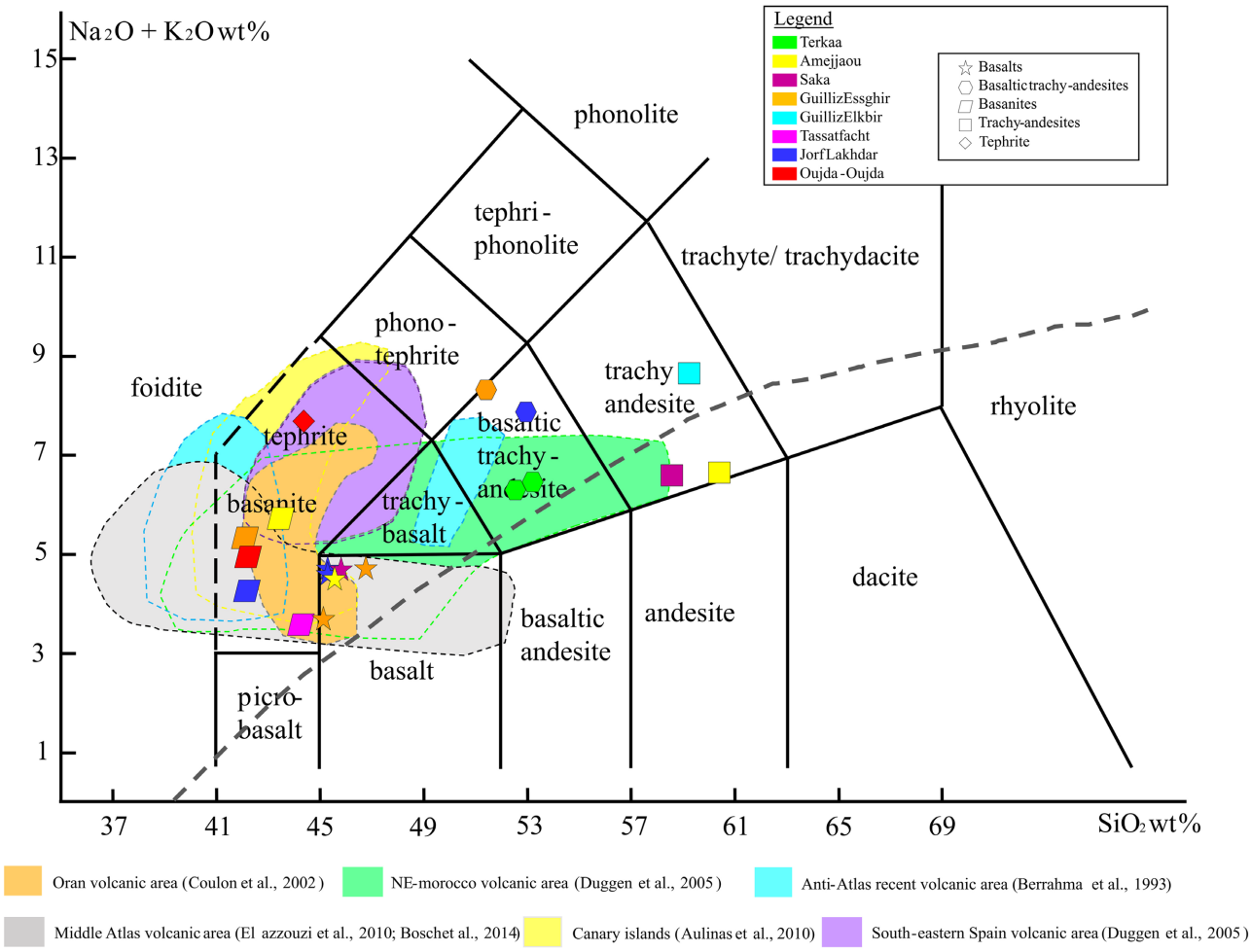


**Figure 15.** TAS diagram of alkali volcanic rock samples used in this paper for study and comparison [55]. The grey dashed line corresponds to alkaline–subalkaline boundary line defined by [56].

$K_2O$ contents and MgO, CaO and $TiO_2$ low contents. The $P_2O_5$ and $Na_2O$ contents decrease significantly with increasing $SiO_2$ content in relation with the crystallization of the apatite; 2) Trachy-andesite samples have lower contents of $TiO_2$, MgO and CaO than the basaltic trachy-andesites and higher contents of $Al_2O_3$ and $K_2O$, while the content of $Na_2O$ and $P_2O_5$ are quite close in both facies (excepting MR-12 that has a very high $Na_2O$ content; 3) basalts have high $Al_2O_3$, MgO, $Na_2O$ and CaO contents, but low $K_2O$, $TiO_2$ and $P_2O_5$ contents. The negative correlation between CaO and $SiO_2$ contents in these samples correlates with the fractional crystallization of clinopyroxene and plagioclase; 4) basanites have high contents of $TiO_2$, MgO, CaO, $Na_2O$ and $P_2O_5$ but low $Al_2O_3$ and $K_2O$ contents, in these samples, the $P_2O_5$ and $Na_2O$ content decreases towards the less saturated samples.

Rare earth elements patterns for the studied volcanic rock show the same pattern, an enrichment in LREEs and a depletion in MREEs and HREEs (**Figure 17**), which is consistent with the general OIB pattern [57].

All the samples exhibit a positive anomaly of Nd, Dy and Tm and a negative

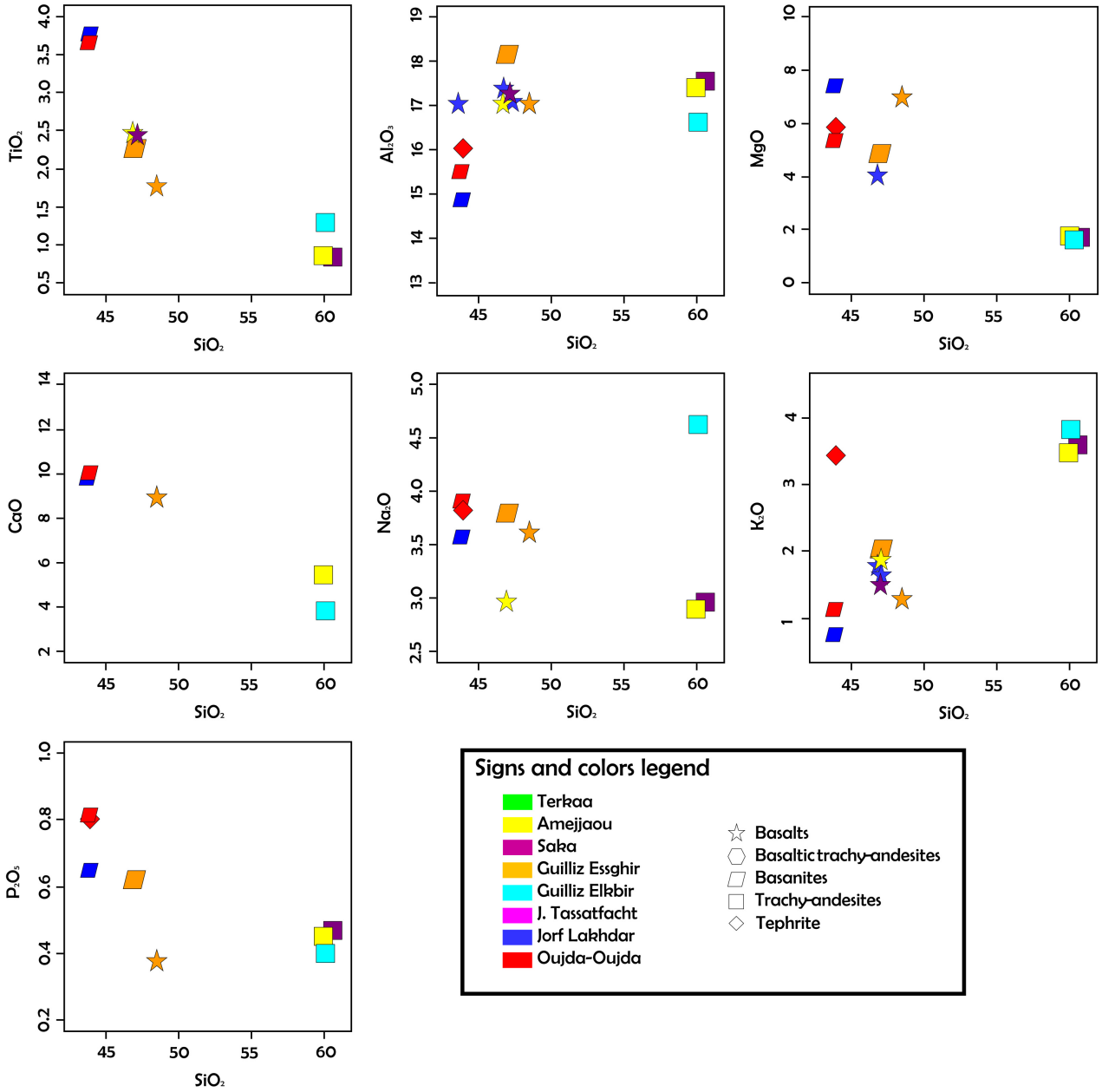


**Figure 16.** Multiple plot of $SiO_2$ vs other major elements ($TiO_2$, $Al_2O_3$, MgO, CaO, $Na_2O$, $K_2O$, $P_2O_5$).

anomaly of Ho and Er. Chondrite-normalized rare earth elements (REE) diagrams show a negative anomaly of Sm, well recorded in Guilliz Essghir samples and of Gd in Jorf Lakhdar, Terkaa and Amejjaou samples. Three samples (MR-12, MR-39 and MR-41) exhibit a very low (Eu/Eu*) of 0.84 - 0.85 while the others show a slight negative and positive Eu anomalies (Eu/Eu* = 0.91 - 1.38). (Ce/Ce*) anomalies are almost steady, with values ranging between (0.86 and 1.01), the ratio values indicates a small interference of oxidation at an early stage. (La/Lu)N and (La/Sm)N ratios are 7.27 - 28.54 and 2.44 - 4.95, respectively (Table 3). They are higher in basanites and tephrite samples, suggesting a late-stage of fractional crystallization from parent magma. (La/Yb)N, (Gd/Yb)N and (La/Gd)N ratios

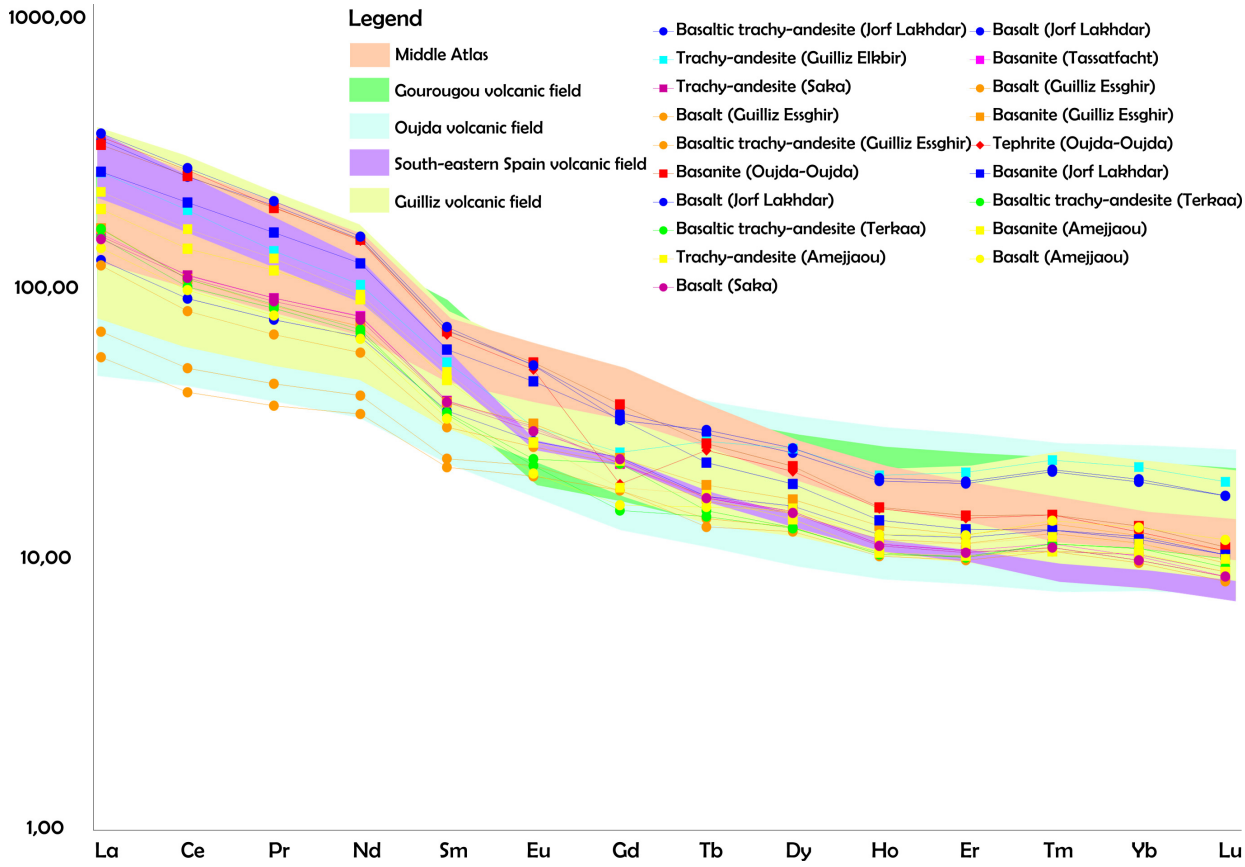


**Figure 17.** REE spider diagram of normalized to chondrite data of the northeast of Morocco (Normalization of [58]).

are 5.29 - 24.5, 1.13 - 2.68 and 2.94 - 16.6, respectively, these values suggest the enrichment of LREE compared to MREE and HREE (Figure 17).

Basalts and basanites show a wide range of concentrations of incompatible elements. Basalts generally have low Zr and Y contents, excepting one sample makes the exception (MR-36) which is very different from other basaltic samples, they also show a low content of Cr, except for two samples (MR-16 and MR-18). Unlike the basalts, basanites show a high content of Zr and Rb, except for one sample (MR-13) which exhibit the lowest content of Rb (Figure 18). Basaltic trachy-andesites show low Ni and Cr contents and high Rb contents (excepting the sample MR-20), they show also low Zr and Y contents (excepting sample MR-7). Trachy-andesites samples show close compositions in Zr, Ba and Rb, however, Ni, Cr and Y content is very low, except for one sample (MR-12), where Y content is notably high. Tephrite sample shows low Ni, Zr, Rb and Cr contents and high Ba and Y contents. The highest concentrations of large-ion lithophile elements (LILEs) such as Rb and Ba, and high-field-strength elements (HFSEs) such as Nb and Zr are those corresponding to Oujda area (Amejjaou and Oujda-Oujda) (Figure 17 & Figure 18).

## 6. Discussion

The Neogene volcanism of Morocco was studied during last decades to understand

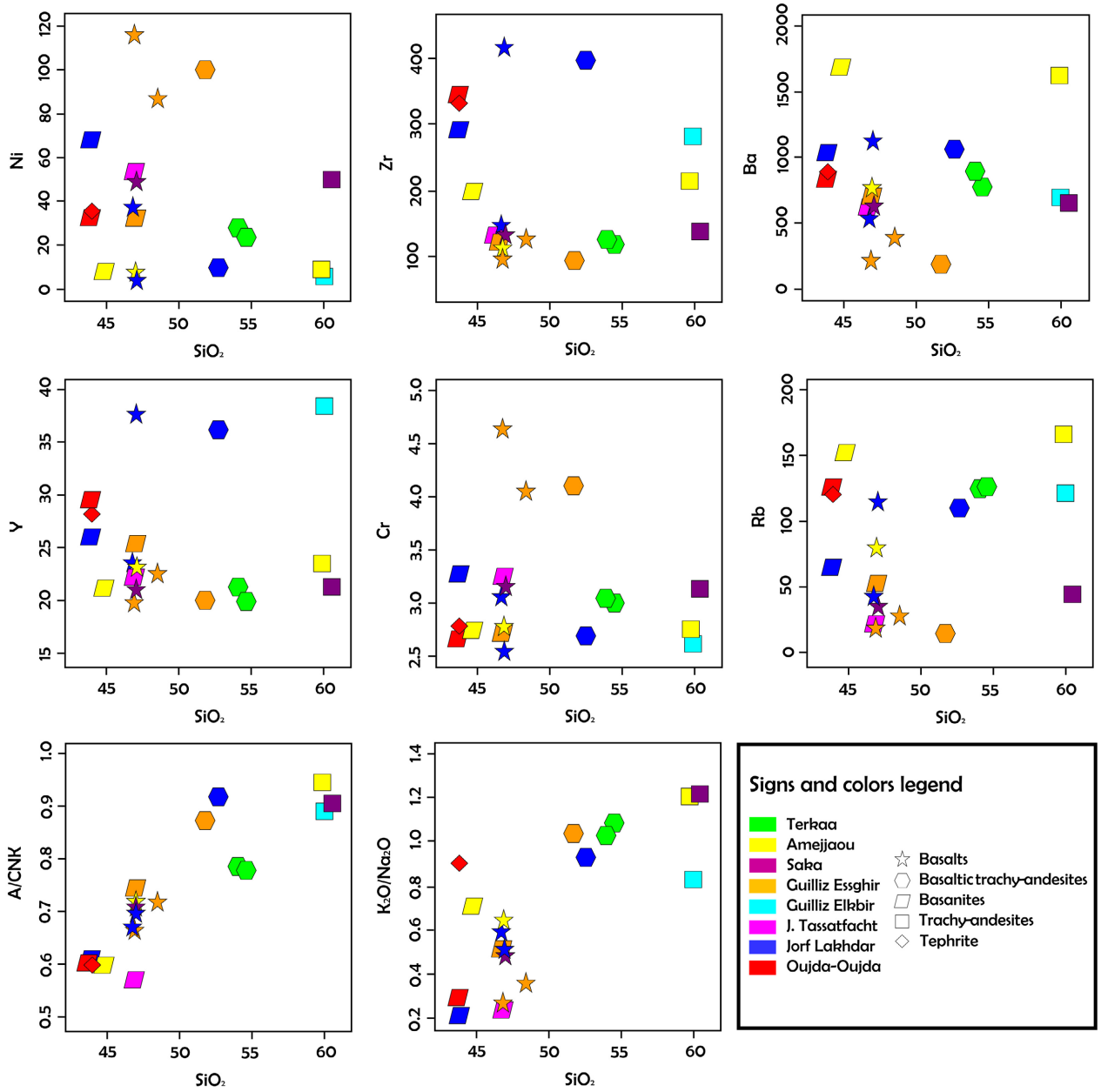


**Figure 18.** Multiple plots of $SiO_2$ vs Ni, Zr, Ba, Rb, Y, Cr, Sr, A/CNK and $K_2O/Na_2O$.

the geodynamic settings of the Western Mediterranean region during this time period, however, most studies were focused mainly on the Miocene volcanic activity, being almost all studies performed on Plio-quaternary activity dealing with the geochronology and the geochemical fingerprints of this activity with no or rare detailed petrographic studies of the Plio-quaternary volcanic rocks. For this reason, this study aims to fill this gap and describe in details the petrography of those rocks. The geochemistry was studied to make a comparison with the previous data of similar rocks from other structural domains in Morocco and in the western Mediterranean region. We therefore choose South-eastern Spain, Oran region in Algeria, Canary Islands, Anti-Atlas and Middle Atlas and pre-

vious studies on North-eastern Morocco. At a global scale, all these volcanic rocks have geochemical signatures similar to those of continental intraplate volcanic settings and OIB (Ocean-Island Basalts). Finally, we try to put our observations within the CiMACI global model.

REEs patterns and the major element concentrations of the alkali olivine basalts are closely comparable to those of average ocean island basalts (OIB) and intra-continental basalts (**Figure 17**). Linear correlations observed in major oxides vs. silica diagrams might indicate that the studied areas have experienced fractionation of Olivine and Clinopyroxene to varying degrees [59]. Phenocrysts of zoned clinopyroxene suggest that a magma mixing has been involved and lead to a more complex evolution model.

The La/Nb classification (based on [8] classification of alkaline, transitional and Calc-alkaline activities, he used the following discriminating rule: Alkaline (for: La/Nb < 1); Transitional (for: 1 < La/Nb < 2) and Calc-alkaline (La/Nb > 2)) shows that three samples represent the Calc-alkaline volcanic activity (Amejjaou), two samples represent the Subalkaline activity (Terkaa), while the Alkaline activity is represented by the majority of samples. The latter mainly consists of basalts and basanites, having a low La/Nb ratios (0.51 - 0.78 except for one sample having a ratio of 0.98) highly supports a HIMU-type OIB basalts [60]. The geochemical signature of the alkalic activity supports an enriched asthenospheric mantle origin, also suggested for Cenozoic Alkali rocks from the volcanic provinces of Central Europe and Western Mediterranean.

Recent volcanism in Oujda area is mainly represented by an alkaline activity, with rocks spanning from basalts to basanites and basaltic trachy-andesites in Jorf Lakhdar; Basanites and tephrites in Semara; Alkali basalts in Oued Lakram; Basanites and tephrites in Oujda-Oujda. For Guilliz volcanic province, the targeted areas were those affected by the latest alkaline activity. It is marked by the presence of basanites in Jbel Tassatfacht; basaltic trachy-andesites in Ezzerga and Jbel Elghassoul; as for the main volcanic area of Guilliz (s.s.), we have identified trachy-andesites in Guilliz Elkbir (which represents the core), while basalts, basaltic trachy-andesites and basanites are represented in Guilliz Essghir. In Nador area, the three volcanic sites have completely different geochemical print. Terkaa volcanic rocks represent the transitional term of the most recent volcanic activity and consist of basaltic trachy-andesites. Selouane is made of alkaline basaltic trachy-andesites. In Amejjaou, the Calc-alkaline trachy-andesites were identified, in addition to basalts and basanites. Saka volcanic area shows a very close petrographic composition to Amejjaou, with the dominance of basalts and trachy-andesites.

The correlations between major and trace elements denote the fractional crystallization of existing phenocryst assemblages (Ol, Cpx and Mt). All the rocks show an enrichment in LREEs and a depletion with tiny variation of MREEs and HREEs and indicate similar pattern of Oceanic Island Basalts (OIB) (**Figure 17**).

Recent volcanic activities in the Mediterranean region show similar petro-

graphic and geochemical characteristics. Below is a brief summary of these characteristics in each of the Anti-Atlas, SE of Spain, Oran, Middle Atlas and NE of Moroccan Plio-quaternary volcanic areas:

Alkali volcanic rocks in the Canary Islands mainly consist of phonolites, tephri-phonolite, phonotephrite, tephrite, basanite and basalts (**Figure 15**). They show different textures (aphanitic, microlitic, trachytic and porphyritic) with a fine groundmass while mineral phases mainly consist of Ol and CPx, in addition to Neph, Pl, Amph, Foides, Ti (Titanite), F.K, Oxy and Ap (Apatite). They exhibit a progressive increase of major elements (*i.e.* CaO, $TiO_2$, FeOt, MgO and $P_2O_5$) suggesting the fractioning of Cpx, Ol and Oxides and the removal of Amph, Pl and the Foides [61].

In southeastern Spain, Alkali volcanic rocks (**Figure 15**) exhibit a phenocryst assemblage consisting of Ol, Cpx and Mt. Geochemical composition show positive Th-U anomalies and show a relative increase of Nb and Ta and decrease of K, Pb, and have a relatively low Rb, Ba, Th, U, K and Pb, and moderately high Sr and Ti concentrations. MgO content correlates negatively with $Al_2O_3$, Ta, Nb, Zr and Hf and positively with $TiO_2$, Cr and Ni [8]. Alkali basalts from Oujda Oued lakram (data from [8]; when we visited the outcrop, it was quite oxidized and could not use any sample for geochemical analysis) and the basaltic andesites of Guilliz area exhibit similar characteristics of alkali volcanic rocks in the SE of Spain.

In Algeria, Alkali volcanic rocks of Oran area in Algeria (**Figure 15**) exhibit a geochemistry similar to the OIB's, with enrichment in LREE and Nb. They show a porphyritic texture with fine-grained groundmass and phenocrysts of Ol, Cpx, Pl, Ap and Oxy. Cpx phenocrysts have a brownish colour and they frequently exhibit a complex zoning with green core, referring to a Ti-rich composition. Foides are occasionally present as interstitial Nephelines and Analcite. The alkali basalts are $TiO_2$-rich and their Mg values indicate both primitive and differentiated terms [7]. These rocks go together with alkaline basaltic rocks from Oujda-Oujda, Jorf Lakhdar, Guilliz Essghir and Saka as they show the same geochemical signature with an enrichment of $TiO_2$ and a $SiO_2$ content less than 52 wt%.

The Alkali volcanic rocks of Saghro outcrops (Anti-Atlas, Morocco) are mostly phonolitic nephelinites to Alkali Phonolites (**Figure 15**) ceasing the eruptive activity. Two volcanic series are distinguished: the main stratovolcano in the center (10 - 6 Ma), consisting of Olivine-bearing nephelinites, tephrites and phonolites; and another volcanic area towards the North, consisting mainly of Olivine-bearing nephelinites (5.5 - 2.8 Ma) [28]. Volcanic facies of Oujda-Oujda outcrop show a great similarity with the phonotephrites of Canary Islands and the phonolites of the Anti-Atlas [28] [61].

The Plio-quaternary alkali and subalkaline volcanic province in the Middle Atlas includes Alkali basalts, basanites and few nephelinites (**Figure 15**). They are Mg-rich and their geochemistry generally exhibit a multi-elements pattern

similar to the primitive basalts [62] and those of intraplate OIB. They show a typical pattern for incompatible elements with enrichment of LREE, increase in Yb to La contents and a negative anomaly in K, Rb and Ba [18]. Basaltic andesite (MR-18) from Guilliz Essghir and the trachy-basalt (MR-34) from Jorf Lakhdar have the most similar geochemical resemblance with the alkali basalts of the Middle Atlas.

In the Northeast of Morocco, our study region, in the alkali volcanic rocks of Gourougou and Guilliz, MgO, Cr and Ni correlate positively, with Ga too in Gourougou volcanic field, and inversely with $Al_2O_3$ in all the volcanic areas, and with $K_2O$ and Th in Gourougou. Some of alkali samples of Gourougou and Guilliz, lack the negative K anomaly. Volcanic rocks of Oujda volcanic field exhibit a decrease in MgO, FeO, $TiO_2$, Co and V and a relative depletion of Rb, Th, U, K and Pb. The MgO correlates positively with CaO, $CaO/Al_2O_3$, Cr and Ni and negatively with $Al_2O_3$, MnO, Cs, Hf, Eu, Yb, Zr, Lu and Y.

### 6.1. Implication of Recent Magmatic Activity of NE of Morocco in CiMACI Global Model of [42]

The Circum Mediterranean Anorogenic Cenozoic Igneous province (CiMACI) refers to the Tertiary anorogenic magmatism, reported widely from the Mediterranean area. Previous studies revealed a common sub-lithospheric mantle source component beneath most of the regions where the anorogenic magmatism has been identified and studied (**Figure 19**); this source is also referred to as

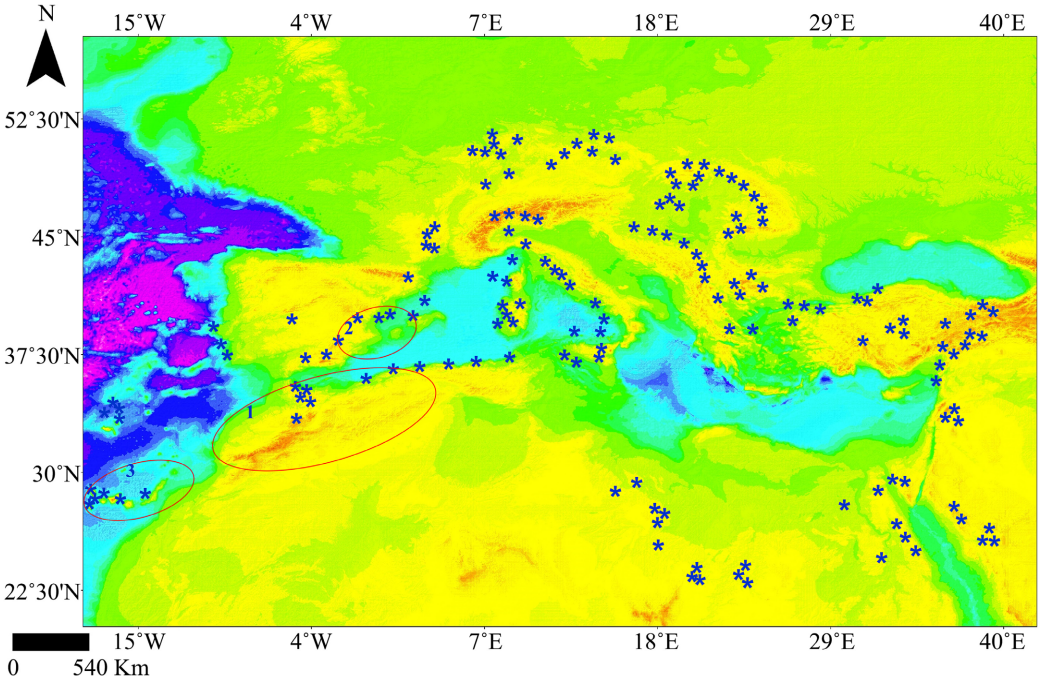


**Figure 19.** Digital topography of circum-Mediterranean area from NOAA (https://ngdc.noaa.gov/mgg/global/global.html) showing the locations of Cenozoic igneous provinces [42]. Red circles refer to the anorogenic provinces discussed in this paper [1: Maghrebian Africa (Morocco and Algeria); 2: Spain; 3: Canary Islands].

the Common Mantle Reservoir (CMR). P and S wave velocity anomalies revealed by different seismic tomography studies beneath CiMACI province and suggest the presence of mantle plumes and diapiric upwellings. CiMACI igneous activity may occur either in extensive settings or in compressive phases as it took place in France along old suture zones affected by Cenozoic rifting and in Turkey in a hinterland position above active or fossil subduction zones. Hence, the term anorogenic cannot be used as an exact synonym of "intra-plate" and the term orogenic cannot be used as synonym of "subduction-related", as both terms are open to encompass a variety of geochemical compositions, unnecessarily related to a contemporaneous geodynamic event [42].

CiMACI rocks are generally effusive and are under-saturated to saturated ($SiO_2$ between 45 and 57 wt%), they are frequently sodic ($Na_2O/K_2O$ between 1.4 - 5) and rarely CaO-rich [4] [63] [64] [65] [66]. The most primitive mafic rocks are under-saturated and alkali-rich ($Na_2O + K_2O$ between 3 and 10 wt%). The main recorded subalkaline lithologies are the basaltic andesites, andesites, picritic basalts, dacites and rhyolites. While the identified alkali rocks are tephrites, tephri-phonolites, leucitites and hauynophyres [67].

Cenozoic magmatic activity in NW Africa is mostly represented by volcanic rocks characterized by a temporal sequence from orogenic products (Miocene Calc-alkaline to high-K Calc-alkaline and Shoshonites) to anorogenic compositions (Plio-quaternary $Na_2O$-rich Alkaline). The anorogenic products generally show typical trace element patterns of magmas emplaced in intraplate settings, such as negative K anomalies, peaks at HFSE (Nb-Ta-Hf-Zr), enrichment of LILE (Cs, Ba, Sr) over HFSE and depletion of Rb [42]. Volcanic rocks with intermediate geochemical affinities between orogenic and anorogenic compositions occur in many areas (e.g., Spain, France, Algeria, Morocco, Turkey) and are undoubtedly related to the interaction between anorogenic sub-lithospheric melts and orogenic subcontinental lithospheric mantle [6] [8].

The geodynamic model of [42] points to a partially melted sub-lithospheric mantle, resulting from different geodynamic settings related to lithospheric extension, and compression, including continental collision and orogenic collapse, contemporaneous subduction, slab roll-back and slab-window formation.

### 6.2. Implication of Recent Magmatic Activity of NE of Morocco in Regional Geodynamic Models

Three models can be proposed to explain the presence of the post-collisional volcanic activity during the Plio-quaternary in NE of Morocco, taking in consideration the regional geodynamic settings within the neighbouring regions. Two of them were previously suggested for NE of Morocco by [6] [8].

The first model investigates the difference in geochemical characteristics of rocks close in age and petrography occurring within the same area. The aim is to explain the temporal transition from an orogenic igneous activity to an anorogenic magmatic activity, e.g., in Maghrebian Africa, Pannonian Basin and Tur-

key (e.g. [6] [7]). It consists of an adiabatic decompression causing partial melting of the asthenosphere as the mantle beneath the slab rises through the slab-window created by the break-off of the subducted slab (**Figure 20(a)**).

The second was proposed by [8] for continental margins of South Iberia and NW of Africa. It suggests that the igneous activity is structurally related to a subduction system. It involves slab rollback or simple lithospheric delamination and steepening of subducted oceanic lithosphere. Those elements contribute in the transport of mantle flow to the surface by creating low-pressures zones

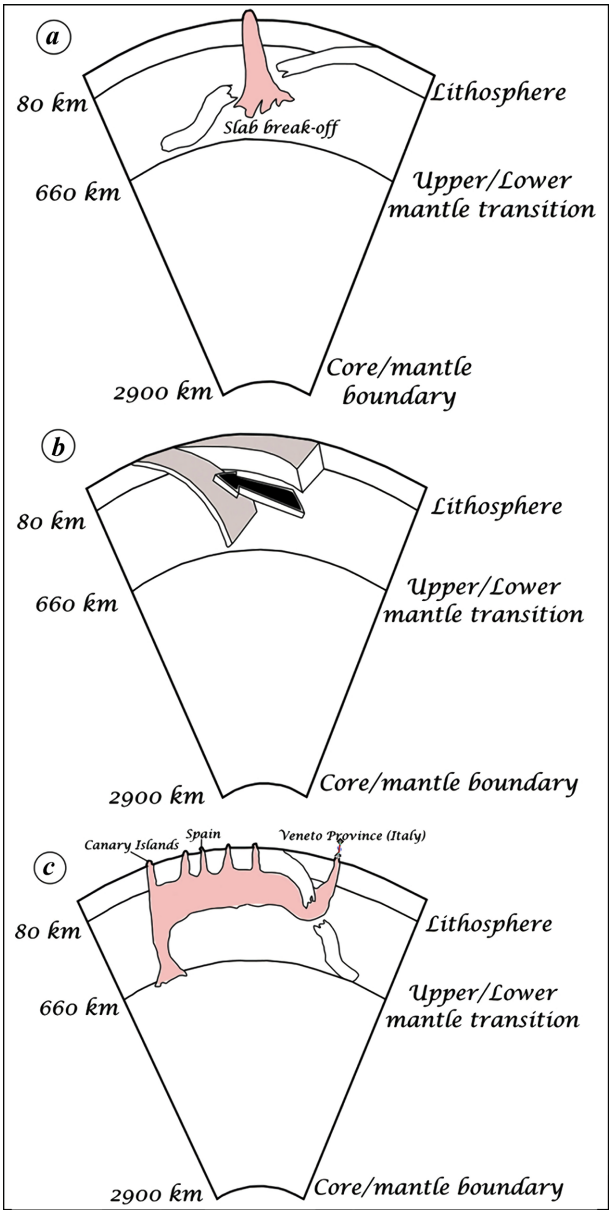


**Figure 20.** Schematic representation of three different petrological and geodynamic models proposed in the literature to explain the origin of individual volcanic districts ((a) Shallow mantle upwelling induced by subducted slab break-off; (b) slab-window causing adiabatic decompression of asthenospheric mantle [71]; (c) Channelized mantle plume along sub-lithospheric weak zones and through a slab-window).

(**Figure 20(b)**). This model stands perfectly with geophysical data (earthquake hypocentres' locations and velocity anomalies) suggesting the presence of a thin wedge-shaped layer (20 - 40 km) with asthenospheric material beneath SE of Spain and NE of Morocco [68] [69].

The third model was proposed to explain the magmatic activity of Veneto Volcanic Province and the north of Pannonian Basin [1] [70] in northern Italy and Central Europe, respectively (**Figure 20(c)**). It consists of a channelized plume sourcing probably for the lower mantle and laterally extending in the asthenosphere, feeding volcanic areas with magmatic flow through the weak zones all along the Mediterranean and beneath the North-African crust during the late Miocene to Quaternary. It also invokes the first model to explain the drastic change in geochemistry of volcanic rocks present within the same areas and are closest in age. This model covers a variety of aspects, represented within this study, including the similarities between the different volcanic provinces, discussed previously, petrographic characteristics and the geochemical evolution of volcanic rocks of NE of Morocco.

In northeastern Morocco, the main magmatic source during late Miocene (Pliocene) changed from a subduction-modified subcontinental lithosphere to a plume-contaminated sublithospheric source. Indeed, some of the silica-saturated samples in Gourougou and Guilliz do not show the expected enrichment and depletion in some FMEs (Fluid-Mobile Elements) (e.g. Th, U, K and Pb) and display large ranges in these elements' ratios, which values indicate a source between OIB and subduction zone lavas. Some alkali under-saturated samples show silent depletion and enrichment in some FMEs (e.g. Th, U, K and Pb). Such behaviour suggests a binary mixing of magmas from different sources, including a shallow mantle wedge, enriched by melts and fluids from subducted oceanic lithosphere beneath the Alboran Basin; a metasomatically enriched subcontinental mantle lithosphere and an upwelling plume-contaminated asthenosphere beneath the south of Iberia and northwest of Africa [6] (**Figure 21**).

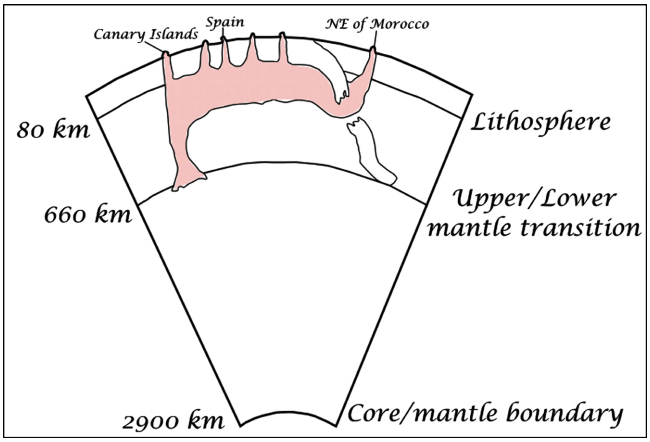


**Figure 21.** Application of the model of [1] in the NE of Morocco; Channelized mantle plume along sub-lithospheric weak zones and through slab-window and setup of NE of Morocco' anorogenic volcanic province.

This change can be observed in the Gourougou stratovolcanic area, in a progressive temporal and geochemical evolution marked by decreasing influence of subduction related component and increasing effect of intraplate-related component.

### 6.3. Conclusions

Petrographic data and geochemical analysis of volcanic rocks from NE of Morocco's Plio-quaternary volcanic fields show the dominance of Na-rich basaltic rocks (basanites, basalts, tephrites and basaltic trachy-andesites), followed by the trachy-andesites. Major and trace element compositions exhibit an enrichment of LILE over HFSE, with high content of Mg and show similar pattern of Oceanic Island Basalts (OIB). The identification and characterization of hydrothermal alteration facies and minerals help us get a better understanding of hydrothermal and geothermal systems, induce thermal parameters and deduce water/rock interaction processes such as the temperature and pH, which will be the main perspective of related studies. We believe that involved hydrothermal fluids in volcanic rocks of NE of Morocco must be at least two different fluids, a low temperature fluid and a high temperature fluid.

Plio-quaternary alkaline volcanic activity, as an anorogenic magmatic province shares many similarities with neighboring anorogenic magmatic areas (e.g. Spain, Algeria, and Morocco), referred as CiMACI province developed along the Mediterranean area. Comparison of different anorogenic magmatic fields within the global model highlighted a great resemblance that supports the idea of areas having a common source beneath the lithosphere. Indeed, inspired from [1], a new model is suggested for the NE of Morocco' recent volcanic province, involving channelized mantle plume along sub-lithospheric weak zones and a slab-window.

## Acknowledgements

Authors would like to thank Mr. Jean Hernandez for his valuable discussions on the early stage of this work, as well as the reviewers for their critical comments.

## Conflicts of Interest

The authors declare no conflicts of interest regarding the publication of this paper.

## References

[1] Harangi, S., Downes, H. and Seghedi, I. (2006) Tertiary-Quaternary Subduction Processes and Related Magmatism in the Alpine-Mediterranean Region. *Geological Society, London, Memoirs*, **32**, 167-190. https://doi.org/10.1144/GSL.MEM.2006.032.01.10

[2] Hernandez, J. (1983) Le volcanisme Miocène du Rif Oriental (Maroc), Géologie, Pétrologie et Minéralogie d'une province shoshonitique. Mémoires des Sciences de la terre, Université pierre et marie curie, Académie de paris.

[3] Coulon, C., Maluski, H., Bollinger, C. and Wang, S. (1986) Mesozoic and Cenozoic Volcanic Rocks from Central and Southern Tibet: $^{39}Ar/^{40}Ar$ Dating, Petrological Characteristics and Geodynamic Significance. *Earth and Planetary Science Letters*, **79**, 281-302. https://doi.org/10.1016/0012-821X(86)90186-X

[4] El Bakkali, S., Gourgaud, A., Bourdier, J.-L., Bellon, H. and Gundogdu, N. (1998) Post-Collision Neogene Volcanism of the Eastern Rif (Morocco): Magmatic Evolution through Time. *Lithos*, **45**, 523-543. https://doi.org/10.1016/S0024-4937(98)00048-6

[5] El Azzouzi, M., Bernard-Griffiths, J., Bellon, H., Maury, R.C., Pique, A., Fourcade, S., Cotten, J. and Hernandez J. (1999) Evolution des sources du volcanisme marocain au cours du Néogène. *Comptes-rendus de l'Académie des Sciences de Paris*, **329**, 95-102. https://doi.org/10.1016/S1251-8050(99)80210-9

[6] Maury, R.C., Fourcade, S., Coulon, C., El Azzouzi, M., Bellon, H., Coutelle, A., Ouabadi, A., Semroud, B., Megartsi, M., Cotton, J., Belanteur, O., Louni-Hacini, A., Pique, A., Capdevila, R., Hernandez, J. and Rehault, J.P. (2000) Post-Collisional Neogene Magmatism of the Mediterranean Maghreb Margin: A Consequence of Slab Breakoff. *Comptes Rendus de l'Académie des Sciences—Series IIA—Earth and Planetary Science*, **331**, 159-173. https://doi.org/10.1016/S1251-8050(00)01406-3

[7] Coulon, C., Megartsi, M., Fourcade, S., Maury, R.C., Bellon, H., Louni-Hacini, A., Cotton, J. and Hermitte, D. (2002) Post-Collision Transition from Calc-Alkaline to Alkaline Volcanism during the Neogene in Oranie (Algeria): Magmatic Expression of a Slab Breakoff. *Lithos*, **62**, 87-110. https://doi.org/10.1016/S0024-4937(02)00109-3

[8] Duggen, S., Hoernle, K., Van Den Bogaard, P. and Garbe-Schönberg, A. (2005) Post-Collisional Transition from Subduction to Intraplate-Type Magmatism in the Westernmost Mediterranean: Evidence for Continental-Edge Delamination of Subcontinental Lithosphere. *Journal of Petrology*, **46**, 1155-1201. https://doi.org/10.1093/petrology/egi013

[9] Hernandez, J. and Bellon, H. (1985) Chronologie K-Ar du volcanisme miocène du Rif oriental (Maroc): Implications tectoniques et magmatologiques. *Revue de géologie dynamique et de géographie physique*, **26**, 85-94.

[10] Hernandez, J., Larouziere, F.D., Bolze, J. and Bordet, P. (1987) Le magmatisme neogene betico rifain et le couloir de décrochement trans-Alboran. *Bulletin de la Société géologique de France*, **8**, 257-267. https://doi.org/10.2113/gssgfbull.III.2.257

[11] Lonergan, L. and White, N. (1997) Origin of the Betic-Rif Mountain Belt. *Tectonics*, **16**, 504-522. https://doi.org/10.1029/96TC03937

[12] Pique, A., Le Roy, P. and Amrhar, M. (1998) Transtensive Synsedimentary Tectonics Associated with Ocean Opening: The Essaouira-Agadir Segment of the Moroccan Atlantic Margin. *Journal of the Geological Society*, **155**, 913-928. https://doi.org/10.1144/gsjgs.155.6.0913

[13] El bakkali, S. (1995) Volcanologie et magmatologie du systeme du gourougou (rif oriental, maroc). Thesis, J.-L. Terre, océan, Espace Clermont-Ferrand 2, 285 p.

[14] Yanev, Y. (1976) Caractère pétrochimique et zonalité du volcanisme néogène-quaternaire du Maroc. *Mines et Géologie*, *Rabat*, **40**, 19-44.

[15] El Azzouzi, M., Maury, R.C., Fourcade, S., Coulon, C., Bellon, H., Ouabadi, A., Semroud, B., Megartsi, M., Cotten, J., Belanteur, A., Louni-Hacini, A., Coutelle, A. Pique, A., Capdevila, R., Hernandez, H. and Rehault, J.-P. (2003) Evolution spatiale et temporelle du magmatisme néogène de la marge septentrionale du Maghreb: Manifestation d'un détachement lithospherique. *Notes et Mémoires du Service*

*Géologique*, **447**, 107-116.

[16] Duggen, S. (2002) Spatial and Temporal Geochemical Evolution of Igneous Rocks in the Alboran Region (Westernmost Mediterreanean): Implications for the Origin of Mediterranean-Style Back-arc Basins and the Messinian Salinity Crisis. Ph.D. Thesis, University of Kiel, Kiel.

[17] Duggen, S., Hoernle, K., Klügel, A., Geldmacher, J., Thirlwall, M.F., Hauff, F., Lowry, D. and Oates, N. (2008) Geochemistry of Miocene Alborán Basin Volcanism. PANGAEA.

[18] El Azzouzi, M., Maury, R.C., Bellon, H., Youbi, N., Cotten, J. and Kharbouch, F. (2010) Petrology and K-Ar Chronology of the Neogene-Quaternary Middle Atlas Basaltic Province, Morocco. *Bulletin de la Société Géologique de France*, **181**, 243-257. https://doi.org/10.2113/gssgfbull.181.3.243

[19] Louni-Hacini, A., Bellon, H., Maury, R.C., Megartsi, M., Coulon, C., Semroud, B., Cotten, J. and Coutelle, A. (1995) Datation $^{40}$K-$^{40}$Ar de la transition du volcanisme calco-alcalin en Oranie au Miocène supérieur. *Comptes Rendus de l'Académie des Sciences Paris*, *série IIa*, **321**, 975-982.

[20] Duggen, S., Hoernle, K., van den Bogaard, P. and Harris, C. (2004) Magmatic Evolution of the Alboran Region: The Role of Subduction in Forming the Western Mediterranean and Causing the Messinian Salinity Crisis. *Earth and Planetary Science Letters*, **218**, 91-108. https://doi.org/10.1016/S0012-821X(03)00632-0

[21] Pearce, J.A., Bender, J.F., De Long, S.E., Kidd, W.S.F., Low, P.J., Güner, Y., Saroglu, F., Yilmaz, Y., Moorbath, S. and Mitchell, J.G. (1990) Genesis of Collision Volcanism in Eastern Anatolia, Turkey. *Journal of Volcanology and Geothermal Research*, **44**, 189-229. https://doi.org/10.1016/0377-0273(90)90018-B

[22] Coulon, C. (1977) Le volcanisme calco-alcalin cénozoïque de Sardaigne (Italie). Pétrographie, géochimie et genèse des laves andésitiques et des ignimbrites. Signification géodynamique. Thèse d'État, université de Marseille, Marseille, 385 p.

[23] Zeck, H.P., Kristensen, A.B. and Williams, I.S. (1998) Post-Collisional Volcanism in a Sinking Slab Setting. Crustal Anatectic Origin of Pyroxeneandesite Magma, Caldear Volcanic Group, Neogene Alboran Volcanic Province, Southeastern Spain. *Lithos*, **45**, 499-522. https://doi.org/10.1016/S0024-4937(98)00047-4

[24] Peccerillo, A. (1999) Multiple Mantle Metasomatism in Centralsouthern Italy: Geochemical Effects, Timing and Geodynamic Implications. *Geology*, **27**, 315-318. https://doi.org/10.1130/0091-7613(1999)027<0315:MMMICS>2.3.CO;2

[25] Missenard, Y., Zeyen, H., Frizon de Lamotte, D., Leturmy, P., Petit, C., Sebrier, M. and Saddiqi, O. (2006) Crustal versus Asthenospheric Origin of Relief of the Atlas Mountains of Morocco. *Journal of Geophysical Research*, **111**, B03401. https://doi.org/10.1029/2005JB003708

[26] Missenard, Y. and Cadoux, A. (2012) Can Moroccan Atlas Lithospheric Thinning and Volcanism Be Induced by Edge-Driven Convection? *Terra Nova*, **24**, 27-33. https://doi.org/10.1111/j.1365-3121.2011.01033.x

[27] Rachdi, H.E.N. (1989) Etude du volcanisme plio-quaternaire du Maroc Central: Pétrographie, géochimie et minéralogie. Comparaison avec des laves types du Moyen Atlas et du Rekkam (Maroc). Thèse Université Laval, Québec, 115 p.

[28] Berrahma, M., Delaloye, M., Faure-Muret, A. and Rachdi, H.E.N. (1993) Premières données géochronologiques sur le volcanisme alcalin du Jbel Saghro, Anti-Atlas, Maroc. *Journal of African Earth Sciences* (*and the Middle East*), **17**, 333-341. https://doi.org/10.1016/0899-5362(93)90077-4

[29] Chalouan, A., Michard, A., El Kadiri, K., Negro, F., Frizon de Lamotte, D., Soto, J.I. and Saddiqi, O. (2008) The Rif Belt. In: Michard, A., Saddiqi, O., Chalouan, A. and Frizon de Lamotte, Eds., *The Geology of Morocco*, Springer, Berlin, 203-302. https://doi.org/10.1007/978-3-540-77076-3_5

[30] Redouane, M., Si Mhamdi, H., Haissen, F., Raji, M. and Sadki, O. (2022) Lineaments Extraction and Analysis Using Landsat 8 (OLI/TIRS) in the Northeast of Morocco. *Open Journal of Geology*, **12**, 333-357. https://doi.org/10.4236/ojg.2022.125018

[31] Sani, F., Zizi, M. and Bally, A.W. (2000) The Neogene—Quaternary Evolution of the Guercif Basin (Morocco) Reconstructed from Seismic Line Interpretation. *Marine and Petroleum Geology*, **17**, 343-357. https://doi.org/10.1016/S0264-8172(99)00058-6

[32] Correia, A., Rimi, A., Zarhloule, Y. and Carneiro, J. (2017) Northeastern Morocco: A High Geothermal Prospect. *Procedia Earth and Planetary Science*, **17**, 746-749. https://doi.org/10.1016/j.proeps.2017.01.003

[33] Wortel, M.J.R. and Spakman, W. (2000) Subduction and Slab Detachment in the Mediterranean-Carpathian Region. *Science*, **290**, 1910-1917. https://doi.org/10.1126/science.290.5498.1910

[34] Roure, F., Casero, P. and Addoum, B. (2012) Alpine Inversion of the North African Margin and Delamination of Its Continental Lithosphere. *Tectonics*, **31**, TC3006. https://doi.org/10.1029/2011TC002989

[35] Nocquet, J.M. and Calais, E. (2004) Geodetic Measurements of Crustal Deformation in the Western Mediterranean and Europe. *Pure & Applied Geophysics*, **161**, 661-681. https://doi.org/10.1007/978-3-0348-7899-9_11

[36] Didon, J., Durand-Delga, M. and Kornprobst, J. (1973) Homologies géologiques entre les deux rives du détroit de Gibraltar. *Bulletin de la Société géologique de France*, *Série* 7, **15**, 77-105. https://doi.org/10.2113/gssgfbull.S7-XV.2.77

[37] Durand-Délga, M. and Fonboté, J.M. (1980) Le cadre structural de la Méditerranée occidentale. 26° congres Géol. Intern. Paris, colloque n° 5 (Les chaînes alpines issues de la Téthis), Mém. B.R.G.M.

[38] Michard, A., Saddiqi, O., Chalouan, A. and Frizon de Lamotte, D. (2008) Continental Evolution: The Geology of Morocco. Springer, Berlin. https://doi.org/10.1007/978-3-540-77076-3

[39] Polyak, B.G., Fernàndez, M., Khutorskoy, M.D., Soto, J.I., Basov, I.A., Comas, M.C., Khain, V.Y., Alonso, B., Agapova, G.V., Mazurova, I.S., Negredo, A., Tochitsky, V.O., Rubio, J., Bogdanov, N.A. and Banda, E. (1996) Component Parts of the World Heat Flow Data Collection. PANGAEA.

[40] Duggen, S., Hoernle, K., Hauff, F., Klügel, A., Bouabdellah, M. and Thirlwall, M.F. (2009) Flow of Canary Mantle Plume Material through a Subcontinental Lithospheric Corridor beneath Africa to the Mediterranean. *Geology*, **37**, 283-286. https://doi.org/10.1130/G25426A.1

[41] Piqué, A. (1999) L'évolution géologique de Madagascar et la dislocation du Gondwana: Une introduction. *Journal African Earth Sciences*, **28**, 919-930. https://doi.org/10.1016/S0899-5362(99)00069-X

[42] Lustrino, M. and Wilson, M. (2007) The Circum-Mediterranean Anorogenic Cenozoic Igneous Province. *Earth-Science Reviews*, **81**, 1-65. https://doi.org/10.1016/j.earscirev.2006.09.002

[43] Ennadifi, Y. (1972) Etude géologique du Prérif oriental et de son avant-pays: Région

comprise entre Mezguitem, A. Zohra et Tizroutine-Maroc. Tectonique. Université Scientifique et Médicale de Grenoble.

[44] Cherotzky, G. (1978) Petrographie du Maroc (Roches éruptions et métamorphiques). Notes Memoires et Services Géologiques Maroc, 266.

[45] Andries, D. and Bellon, H. (1989) Age isotopique $^{40}$Ar du volcanisme alcalin Neogene d'Oujda (Maroc Oriental) et implications tectoniques. *Sciences Géologiques, bulletins et mémoires*, **84**, 107-116.

[46] Zhang, C., Zhang, L., Bader, T., Song, S. and Lou, Y. (2013) Geochemistry and Trace Element Behaviors of Eclogite during Its Exhumation in the Xitieshan terrane, North Qaidam UHP Belt, NW China. *Journal of Asian Earth Sciences*, **63**, 81-97. https://doi.org/10.1016/j.jseaes.2012.09.021

[47] Steiner, A. (1977) The Wairakei Geothermal Area, North Island, New Zealand. New Zealand Geological Survey Bulletin 90, Wellington.

[48] Boursier, H. (1983) Zoneographie des minéraux hydrothermaux dans les champs géothermiques. Exemple: Les champs des Philippines. Thèse 3e cycle, Orsay, 319 p.

[49] Pozo, M. and Calvo, J.P. (2018) An Overview of Authigenic Magnesian Clays. *Minerals*, **8**, 520. https://doi.org/10.3390/min8110520

[50] Dill, H.G. (2020) A Geological and Mineralogical Review of Clay Mineral Deposits and Phyllosilicate Ore Guides in Central Europe—A Function of Geodynamics and Climate Change. *Ore Geology Reviews*, **119**, Article ID: 103304. https://doi.org/10.1016/j.oregeorev.2019.103304

[51] Seber, D., Barazangi, M., Ibenbrahim, A. and Demnati, A. (1996) Geophysical Evidence for Lithospheric Delamination beneath the Alboran Sea and Rif-Betic Mountains. *Nature*, **379**, 785-790. https://doi.org/10.1038/379785a0

[52] Patrier, P., Papapanagiotou, P., Beaufort, D., Traineau, M., Bril, H. and Ross, J. (1996) Role of Permeability versus Temperature in the Distribution of the Fine (< 0.2 pm) Clay Fraction in the Chipilapa Geothermal System (El Salvador, Central America). *Journal of Volcanology and Geothermal Research*, **12**, 101-120. https://doi.org/10.1016/0377-0273(95)00078-X

[53] Fulignati, P. (2020) Clay Minerals in Hydrothermal Systems. *Minerals*, **10**, 919. https://doi.org/10.3390/min10100919

[54] Kruse, F.A., Bedell, R.L., Taranik, J.V., Peppin, W.A., Weatherbee, O. and Calvin, W.M. (2012) Mapping Alteration Minerals at Prospect, Outcrop and Drill Core Scales Using Imaging Spectrometry. *International Journal of Remote Sensing*, **33**, 1780-1798. https://doi.org/10.1080/01431161.2011.600350

[55] Le Bas, M.J., Le Maitre, R.W., Streckeisen, A. and Zanettin, B. (1986) A Chemical Classification of Igneous Rocks Based on the Total Alkali-Silica Diagram. *Journal of Petrology*, **27**, 745-750. https://doi.org/10.1093/petrology/27.3.745

[56] Miyashiro, A. (1978) Nature of Alkalic Volcanic Rock Series. *Contributions to Mineralogy and Petrology*, **66**, 91-104. https://doi.org/10.1007/BF00376089

[57] Sun, S.S. and McDonough, W.F. (1989) Chemical and Isotopic Systematics of Oceanic Basalts: Implications for Mantle Com-Position and Processes. *Geological Society, London, Special Publications*, **42**, 313-345. https://doi.org/10.1144/GSL.SP.1989.042.01.19

[58] McDonough, W.F. and Sun, S.S. (1995) The Composition of the Earth. *Chemical Geology*, **120**, 223-253. https://doi.org/10.1016/0009-2541(94)00140-4

[59] Wilson, M. (1989) Igneous Petrogenesis: A Global Tectonic Approach. Unwin Hyman, London, 466 p. https://doi.org/10.1007/978-1-4020-6788-4

[60] Weaver, B.L. (1991) Trace Element Evidence for the Origin of Ocean Island Basalts. *Geology*, **19**, 123-126. https://doi.org/10.1130/0091-7613(1991)019<0123:TEEFTO>2.3.CO;2

[61] Aulinas, M., Gimeno, D., Fernandez-Turiel, J.L., Perez-Torrado, F.J., Rodriguez-Gonzalez, A. and Gasperini, D. (2010) Small-Scale Mantle Heterogeneity on the Source of the Gran Canaria (Canary Islands) Pliocene-Quaternary Magmas. *Lithos*, **119**, 377-392. https://doi.org/10.1016/j.lithos.2010.07.016

[62] Villemant, B., Jaffrezic, H., Joron, J.L. and Treuil, M. (1981) Distribution Coefficients of Major and Trace-Elements—Fractional Crystallization in the Alkali Basalt Series of Chaine Des-Puys (Massif Central, France). *Geochimica et Cosmochimica Acta*, **45**, 1997-2016. https://doi.org/10.1016/0016-7037(81)90055-7

[63] Riley, S.J., De Gloria, S.D. and Elliot, R. (1999) A Terrain Ruggedness Index That Quantifies Topographic Heterogeneity. *Intermountain Journal of Sciences*, **5**, 23-27.

[64] Ibhi, A. (2002) Intervention of Carbonate Components in Petrogenesis of the Pyroxene Nephelinites from the Jbel Saghro (Anti-Atlas, Morocco). *Bulletin de la Société Géologique de France*, **173**, 37-43. https://doi.org/10.2113/173.1.37

[65] Conticelli, S., Manetti, P. and Menichetti, S. (1992) Petrology, Chemistry, Mineralogy and Sr-Isotopic Features of Pliocenic Orendites from South Tuscany: Implications on Their Genesis and Evolutions. *European Journal of Mineralogy*, **4**, 1359-1375. https://doi.org/10.1127/ejm/4/6/1359

[66] Stoppa, F., Lloyd, F. and Rosatelli, G. (2003) $CO_2$ as the Virtual Propellant of Carbonatite-Kamafugite Conjugate Pairs and the Eruption of Diatremic Tuffisite Period. *Mineral*, **72**, 205-222.

[67] Mann, P., Escalona, A. and Verónica, M. (2006) Regional Geologic and Tectonic Setting of the Maracaibo Supergiant Basin, Western Venezuela. *AAPG Bulletin*, **90**, 445-477. https://doi.org/10.1306/10110505031

[68] Hoernle, K., Zhang, Y.S. and Graham, D. (1995) Seismic and Geochemical Evidence for Large-Scale Mantle Upwelling beneath the Eastern Atlantic and Western and Central Europe. *Nature*, **374**, 34-39. https://doi.org/10.1038/374034a0

[69] Shuguang, S., Li, S., Yaoling, N., Lifei, Z. and Guibing, Z. (2007) Petrological and Geochemical Constraints on the Origin of Garnet Peridotite in the North Qaidam Ultrahigh-Pressure Metamorphic Belt, Northwestern China. *Lithos*, **96**, 243-265. https://doi.org/10.1016/j.lithos.2006.09.017

[70] Macera, P., Gasperini, D., Piromallo, C., Blichert-Toft, J., Bosch, D., Del Moro, A. and Martin, S. (2003) Geodynamic Implications of Deep Mantle Upwelling in the Source of Tertiary volcanics from the Veneto Region (Southern-Eastern Alps). *Journal of Geodynamics*, **36**, 563-590. https://doi.org/10.1016/j.jog.2003.08.004

[71] Gvirtzman, Z. and Nur, A. (1999) Plate Detachment, Asthenosphere Upwelling, and Topography across Subduction Zones. *Geology*, **27**, 563-566. https://doi.org/10.1130/0091-7613(1999)027<0563:PDAUAT>2.3.CO;2